Cell Stem Cell

Article

Relayed signaling between mesenchymal progenitors and muscle stem cells ensures adaptive stem cell response to increased mechanical load

Graphical abstract

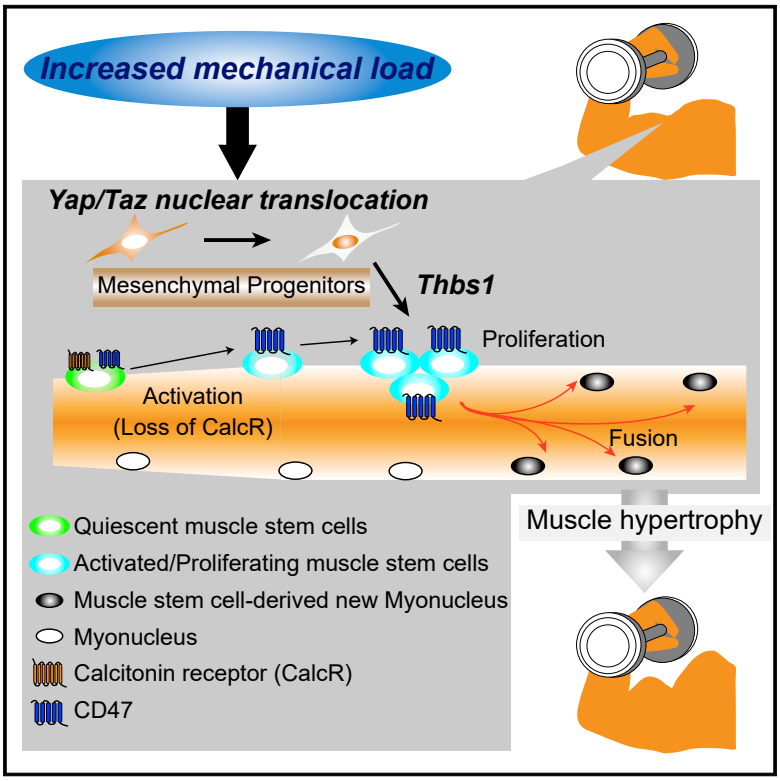

Authors

Akihiro Kaneshige, Takayuki Kaji, Lidan Zhang, ..., Thomas Braun, Akiyoshi Uezumi, So-ichiro Fukada

Correspondence

uezumi@tmig.or.jp (A.U.), fukada@phs.osaka-u.ac.jp (S.-i.F.)

In brief

Kaneshige et al. revealed that initiation of muscle stem cell (MuSC) proliferation in overloaded muscles depends on YAP/TAZ activity in mesenchymal progenitors (MPs). Inactivation of YAP/TAZ in MPs or ablation of MPs blunts myonuclear accretion after mechanical loading. The crosstalk between MPs and MuSCs is mediated via the Thbs1-CD47 axis.

Highlights

- Yap/Taz in mesenchymal progenitor cells of loaded muscles induce MuSC proliferation
- Expression of Thbs1 in mesenchymal progenitors during overload depends on Yap/Taz
- The Thbs1-CD47 axis regulates MuSC proliferation in overloaded muscles
- CD47 activation induces MuSC proliferation in calcitonin receptor mutant muscles

Kaneshige et al., 2022, Cell Stem Cell *29*, 1–16
February 3, 2022 © 2021 The Author(s). Published by Elsevier Inc.
https://doi.org/10.1016/j.stem.2021.11.003

CellPress

Please cite this article in press as: Kaneshige et al., Relayed signaling between mesenchymal progenitors and muscle stem cells ensures adaptive stem cell response to increased mechanical load, Cell Stem Cell (2021), https://doi.org/10.1016/j.stem.2021.11.003

Cell Stem Cell

CellPress
OPEN ACCESS

Article

Relayed signaling between mesenchymal progenitors and muscle stem cells ensures adaptive stem cell response to increased mechanical load

Akihiro Kaneshige,[1,2,3] Takayuki Kaji,[1] Lidan Zhang,[1] Hayato Saito,[1] Ayasa Nakamura,[1] Tamaki Kurosawa,[4,6] Madoka Ikemoto-Uezumi,[4] Kazutake Tsujikawa,[3] Shigeto Seno,[5] Masatoshi Hori,[6] Yasuyuki Saito,[7] Takashi Matozaki,[7] Kazumitsu Maehara,[8] Yasuyuki Ohkawa,[8] Michael Potente,[9,10,11] Shuichi Watanabe,[12] Thomas Braun,[12] Akiyoshi Uezumi,[4,*] and So-ichiro Fukada[1,13,*]

[1]Project for Muscle Stem Cell Biology, Graduate School of Pharmaceutical Sciences, Osaka University, 1-6 Yamada-oka, Suita, Osaka 565-0871, Japan
[2]Biological/Pharmacological Research Laboratories, Central Pharmaceutical Research Institute, Japan Tobacco Inc., 1-1 Murasaki-cho, Takatsuki, Osaka 569-1125, Japan
[3]Laboratory of Molecular and Cellular Physiology, Graduate School of Pharmaceutical Sciences, Osaka University, 1-6 Yamada-oka, Suita, Osaka 565-0871, Japan
[4]Muscle Aging and Regenerative Medicine, Tokyo Metropolitan Institute of Gerontology, 35-2 Sakae-cho, Itabashi, Tokyo 173-0015, Japan
[5]Department of Bioinformatic Engineering, Graduate School of Information Science and Technology, Osaka University, 1-5 Yamada-oka, Suita, Osaka 565-0871, Japan
[6]Laboratory of Veterinary Pharmacology, Department of Veterinary Medical Sciences, Graduate School of Agriculture and Life Sciences, Tokyo University, 1-1-1 Yayoi, Bunkyo-ku, Tokyo 113-8657, Japan
[7]Division of Molecular and Cellular Signaling, Department of Biochemistry and Molecular Biology, Kobe University Graduate School of Medicine, Kobe 650-0017, Japan
[8]Division of Transcriptomics, Medical Institute of Bioregulation, Kyushu University, Fukuoka 812-8582, Japan
[9]Angiogenesis & Metabolism Laboratory, Max Planck Institute for Heart and Lung Research, 61231 Bad Nauheim, Germany
[10]Berlin Institute of Health at Charité (BIH) — Universitätsmedizin Berlin, 13125 Berlin, Germany
[11]Max Delbrück Center for Molecular Medicine in the Helmholtz Association (MDC), 13125 Berlin, Germany
[12]Department of Cardiac Development and Remodeling, Max Planck Institute for Heart and Lung Research, 61231 Bad Nauheim, Germany
[13]Lead contact
*Correspondence: uezumi@tmig.or.jp (A.U.), fukada@phs.osaka-u.ac.jp (S.-i.F.)
https://doi.org/10.1016/j.stem.2021.11.003

SUMMARY

Adaptation to mechanical load, leading to enhanced force and power output, is a characteristic feature of skeletal muscle. Formation of new myonuclei required for efficient muscle hypertrophy relies on prior activation and proliferation of muscle stem cells (MuSCs). However, the mechanisms controlling MuSC expansion under conditions of increased load are not fully understood. Here we demonstrate that interstitial mesenchymal progenitors respond to mechanical load and stimulate MuSC proliferation in a surgical mouse model of increased muscle load. Mechanistically, transcriptional activation of Yes-associated protein 1 (Yap1)/transcriptional coactivator with PDZ-binding motif (Taz) in mesenchymal progenitors results in local production of thrombospondin-1 (Thbs1), which, in turn, drives MuSC proliferation through CD47 signaling. Under homeostatic conditions, however, CD47 signaling is insufficient to promote MuSC proliferation and instead depends on prior downregulation of the Calcitonin receptor. Our results suggest that relayed signaling between mesenchymal progenitors and MuSCs through a Yap1/Taz-Thbs1-CD47 pathway is critical to establish the supply of MuSCs during muscle hypertrophy.

INTRODUCTION

Skeletal muscle is an essential organ for locomotion, metabolism, and life activities. Its plasticity is reflected by an unparalleled ability to adapt to external and internal physiological alterations. For example, enhanced mechanical load induces skeletal muscle remodeling and, consequently, increasing muscle mass and strength, known as muscle hypertrophy. Hypertrophy goes along with enhanced protein synthesis and an increase in myonuclei (Bamman et al., 2018), with the latter being completely dependent on muscle stem (satellite) cells (MuSCs) (Egner et al., 2016; McCarthy et al., 2011). Although a few studies suggested that MuSCs are less important during the early phase of hypertrophy (Murach et al., 2017), the majority of studies

This is an open access article under the CC BY license (http://creativecommons.org/licenses/by/4.0/).

indicate an essential role of MuSCs for efficient muscle hypertrophy, either by myonuclear accretion or as a source of paracrine factors (Egner et al., 2016; Fry et al., 2017; Fukuda et al., 2019; Goh and Millay, 2017; Moriya and Miyazaki, 2018). Although the molecular mechanisms regulating MuSC behavior are critical for muscle hypertrophy, they remain poorly investigated. Because MuSCs are located on contracting and relaxing myofibers, it has been assumed that MuSCs sense changes in myofiber activity. However, MuSCs seem to ignore the basal activity of skeletal muscle and remain in a quiescent state. MuSCs are activated and expand only when skeletal muscle is exposed to a strong mechanical stimulus. At present, it is unknown how increased mechanical load switches MuSCs from quiescence to activation. Myofiber injuries might be one possible trigger for expansion of MuSCs under increased mechanical load (Ebbeling and Clarkson, 1989). However, massive damage or even death of myofibers, required for massive expansion of MuSCs, does not occur in overloaded muscles (Darr and Schultz, 1987; Fukada et al., 2020). Other mechanisms, such as edema formation (swelling caused by excess fluid), responsible for early weight gain of muscles during resistance training, and microfractures of the sarcolemma are more likely signals (Damas et al., 2018; Fukada et al., 2020). In addition, myofiber-derived factors that are released during enhanced mechanical load may contribute to expansion of MuSCs (Guerci et al., 2012; Serrano et al., 2008). Nevertheless, and despite much work on the relationship between mechanical loading and MuSC proliferation, our understanding of these processes is immature, and research questions remain.

It has been assumed that myofibers are primarily responsive for sensing enhanced mechanical load in skeletal muscle, although interstitial mesenchymal cells might be involved as well. Mesenchymal progenitors (Uezumi et al., 2010), also known as fibro/adipogenic progenitors (FAPs) (Joe et al., 2010), are characterized by expression of platelet-derived growth factor receptor alpha (Pdgfrα) and are responsible for pathological fibrosis and fat accumulation in skeletal muscle (Joe et al., 2010; Uezumi et al., 2010, 2011). On the other hand, mesenchymal progenitors are also involved in homeostasis and regeneration of skeletal muscle (Joe et al., 2010; Lemos et al., 2015; Uezumi et al., 2021; Wosczyna et al., 2019). However, knowledge about the role of mesenchymal progenitors in regulation of muscle hypertrophy is lacking.

Yes-associated protein 1 (Yap1) and transcriptional coactivator with PDZ-binding motif (Taz, also known as Wwtr1), are well-known effectors of the Hippo kinase cascade, required for proliferation, survival, and tumorigenesis in many cell types (Yu et al., 2015). Yap1/Taz also function as sensors and transducers of mechanical signals (Dupont et al., 2011), which might important for induction of muscle hypertrophy by mechanical load. In fact, overexpression of YAP induces muscle hypertrophy (Goodman et al., 2015; Watt et al., 2015). However, total Yap1 and phosphorylated Yap1 levels peak only 7 days after onset of surgical overload in FVB/N mice, much later compared with mTORC1 signaling, which peaks 2 days after induction of overload (Goodman et al., 2015). We found previously that Yap1 accumulates in nuclei of calcitonin receptor (CalcR) mutant MuSCs and demonstrated that the CalcR-protein kinase A axis suppresses Yap1 activity in quiescent MuSCs (Zhang et al., 2019). CalcR mutant and constitutively active Yap1-expressing MuSCs (Tremblay et al., 2014) did not exhibit substantial cell division as in overloaded muscle. These results suggest that Yap1 does not have a primary function in myofibers and MuSCs, arguing for an alternative mechanism that is required to induce MuSC expansion in response to increased mechanical load.

Here we investigated the role of mesenchymal progenitors for proliferation of MuSC in overloaded muscle. We further analyzed the role of Yap1/Taz in these cells and assessed their effect on MuSC expansion during increased mechanical load.

RESULTS

Mesenchymal progenitors are essential for myonuclear accretion from muscle stem cells in overloaded muscle

We speculated that Pdgfrα$^+$ mesenchymal progenitors (hereafter Pα$^+$ cells) have a previously underappreciated function in muscle hypertrophy. Therefore, we studied Pα$^+$ cells in overloaded muscles in which the distal tendons of the *gastrocnemius* and *soleus* muscles were cut (tenotomy) to induce compensatory hypertrophy in the *plantaris* (PLA) muscle with little degenerative damage to myofibers (Fukuda et al., 2019). Proliferating Pα$^+$ cells on days 2, 4, and 7 after tenotomy were counted after labeling with 5-ethynyl-2′-deoxyuridine (EdU) or staining against an activation/proliferation marker, Ki67, in *Pdgfra-H2B-EGFP* (*Pa-EGFP*) or C57BL/6 mice (Figure 1A). Two and 4 days after tenotomy, approximately 2% and 13% of Pα$^+$ cells were positive for EdU, and 5% and 30% of Pα$^+$ cells were positive for Ki67, respectively (Figures 1B, 1C, S1A, and S1B). Only a few Pα$^+$ cells were labeled with EdU 6–7 days after tenotomy, and approximately 3% of Pα$^+$ cells expressed Ki67 on day 7 after tenotomy (Figures 1B and 1C). The number of Pα$^+$ cells was increased slightly on day 4 (1.6-fold) and 7 days (2-fold) after tenotomy in *Pa-EGFP* (Figure 1D). The same increase was also detected in C57BL/6 mice 7 days after tenotomy (Figure S1C). In addition, similar to MuSCs, the cell size and granularity of Pα$^+$ cells in fluorescence-activated cell sorting (FACS) analyses were increased 2 days after tenotomy, (Figures 1E, 1F, S1D, and S1E). During this period, apoptotic Pα$^+$ cells were not detected (Figure S1F), indicating that Pα$^+$ cells are activated in response to increased mechanical load and show a transient and moderate increase in proliferation.

To determine the role of activated Pα$^+$ cells in overloaded muscles, we depleted Pα$^+$ cells by treating *Pdgfra^{CreERT}::Rosa^{DTA}* (Pα-DTA) mice with tamoxifen and confirmed successful depletion of Pα$^+$ cells (Figure S2A), as reported previously (Uezumi et al., 2021). Next, PLA muscle hypertrophy was induced in Pα$^+$ cell-deficient mice by tenotomy, followed by EdU injections (Figures 2A). Although the sham muscle weight was decreased by Pα$^+$ cell depletion, correlating with our previous study (Figure S2B), the increased ratio of overloaded muscle weight to sham muscle weight was similar in control (*Pdgfra$^{CreERT/+}$*) and Pα-DTA mice 7 days after tenotomy (Figure 2B), suggesting that early responses, including edema, were similar in control and Pα-DTA mice. However, ablation of Pα$^+$ cells suppressed the increase in total myonuclei after tenotomy (Figure 2C). Likewise, newly formed EdU$^+$ myonuclei were reduced markedly in Pα-DTA compared with control mice (Figures 2D and 2E). M-cadherin (M-cad)$^+$ and M-cad$^+$EdU$^+$ cells

Please cite this article in press as: Kaneshige et al., Relayed signaling between mesenchymal progenitors and muscle stem cells ensures adaptive stem cell response to increased mechanical load, Cell Stem Cell (2021), https://doi.org/10.1016/j.stem.2021.11.003

CellPress
OPEN ACCESS

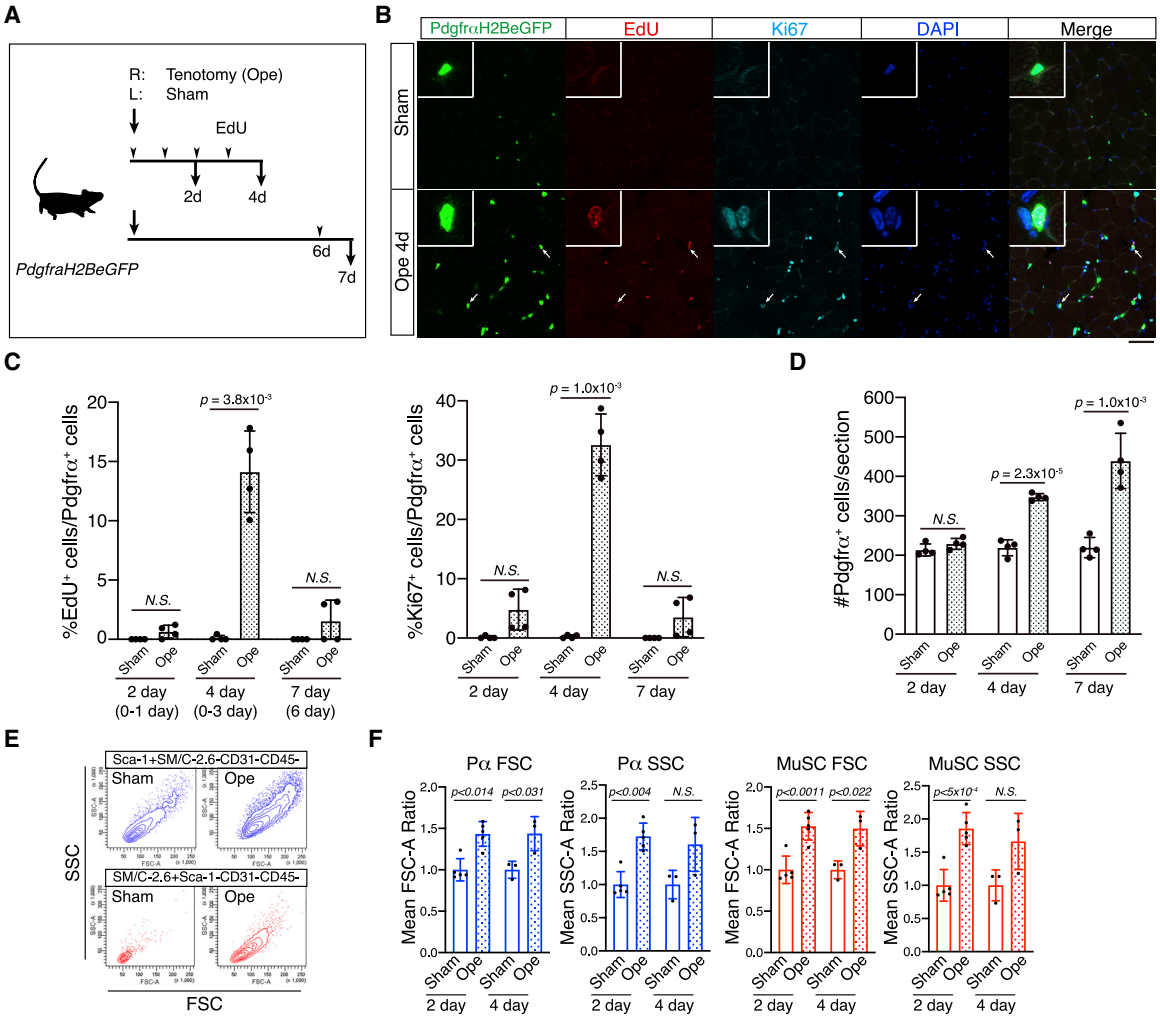

Figure 1. Mesenchymal progenitor cells become activated in overloaded muscle

(A) Experimental scheme for analyzing mesenchymal progenitors in PLA muscle in *Pa-EGFP* on day 2 (n = 4; 2 male [M], 2 female [F]), 4 (n = 4; 2 M, 2 F), and 7 (n = 4; 2 M, 2 F) after tenotomy (Ope; R, right). The contralateral left PLA muscle was used as sham Cont (L, Sham).

(B) Immunostaining of EdU and Ki67 in Sham or Ope muscles on day 4 after tenotomy. Nuclei of Pdgfrα$^+$ cells were labeled with EGFP. Arrows indicate EGFP$^+$EdU$^+$Ki67$^+$ cells. Scale bar, 50 μm.

(C) Percentage of EGFP$^+$EdU$^+$ (left) or EGFP$^+$Ki67$^+$ (right) cells per EGFP$^+$ cells in Sham and Ope muscles of *Pa-EGFP* on days 2, 4, and 7 after tenotomy. The number in parentheses refer to the day of EdU injections.

(D) Number of EGFP$^+$ cells per muscle section on days 2, 4, and 7 after tenotomy.

(E) FACS profiles of mesenchymal progenitors (top) or MuSCs (bottom) from Sham (left) or Ope (right) muscles of C57BL/6 mice, respectively. All profiles show the cell size (FSC) and cell granularity (SSC).

(F) Mean FSC and SSC of mesenchymal progenitors (n = 3–5) or MuSC (n = 3–5).

In all Figures excluding Figure 5G, one symbol means the result of one mouse. All data are presented as mean ± SD. N.S., not significant. Nuclei were counterstained with DAPI. See also Figure S1.

in loaded muscles were also reduced in Pα-DTA mice (Figures 2F and 2G). Because approximately 20% of Pα$^+$ cells survive in Pα-DTA mice (Figure S2A), we assume that the remaining Pα$^+$ cells are sufficient to promote accretion of some MuSC-derived EdU$^+$ nuclei into myofibers.

To further investigate the effects caused by loss of Pα$^+$ cells on MuSCs in overloaded muscles, single myofibers were isolated from overloaded PLA muscle, and Pax7$^+$ cells numbers were counted on day 4, 7, and 10 after tenotomy (Figure 2H). Consistent with the results of myonuclear accretion, the numbers of Pax7$^+$ cells in the overloaded muscle of Pα-DTA mice were reduced remarkably compared with the control 4–10 days after tenotomy (Figure 2I). To elucidate the role of Pα$^+$ cells in MuSC activation, we compared the expression of Ki67 and MyoD between control and Pα-DTA mice. Our previous study indicated that, upon MuSC activation, Ki67 expression occurs 2–4 days after tenotomy and that 60%–80% of MuSCs are Ki67$^+$ on day 4. In addition, the majority of MuSCs proliferate without apparent expression of MyoD (Fukuda et al., 2019). Therefore, we used expression of Ki67, but not MyoD, as a marker for MuSC

Please cite this article in press as: Kaneshige et al., Relayed signaling between mesenchymal progenitors and muscle stem cells ensures adaptive stem cell response to increased mechanical load, Cell Stem Cell (2021), https://doi.org/10.1016/j.stem.2021.11.003

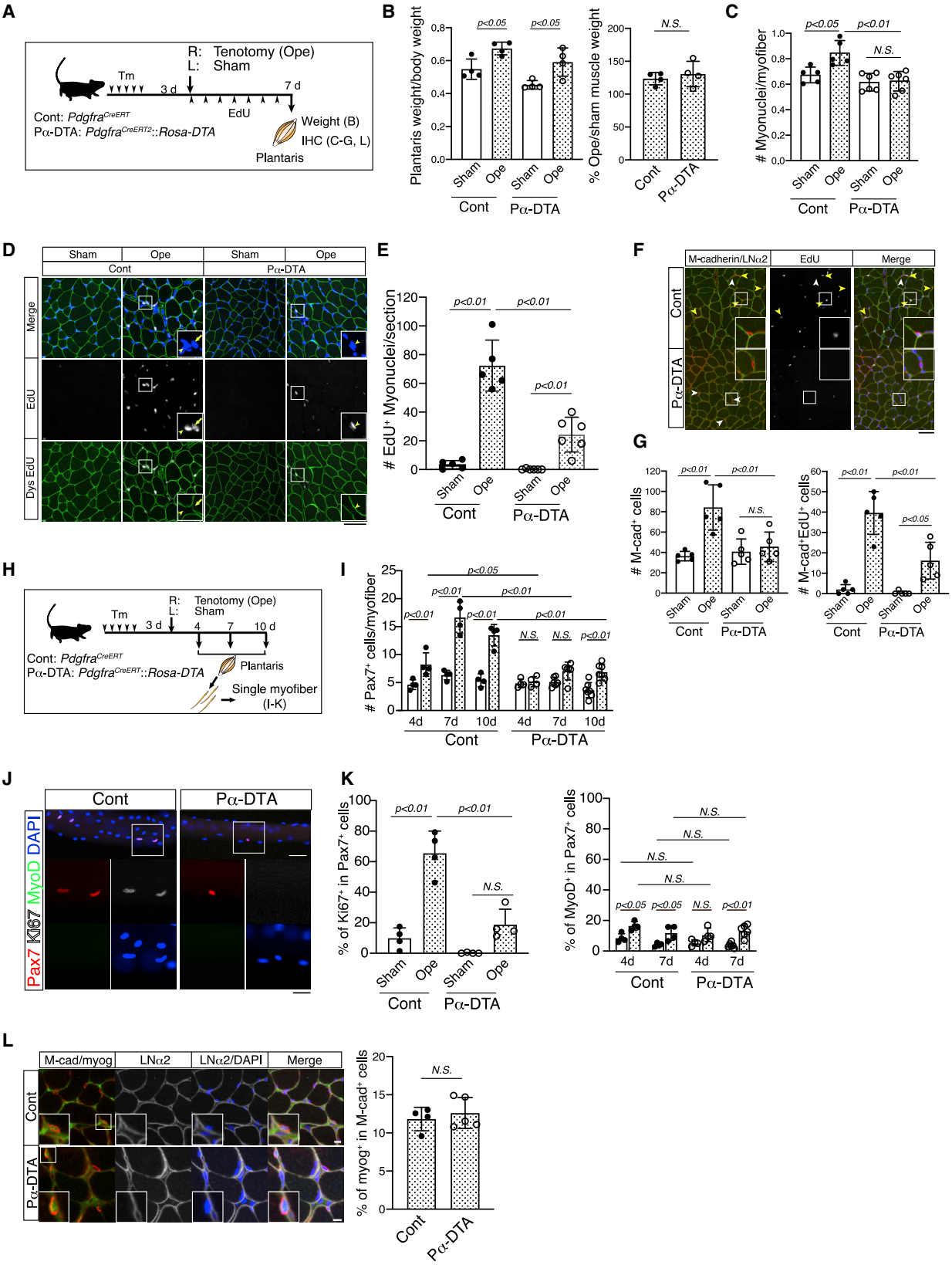

(legend on next page)

activation 4 days after tenotomy. Notably, Ki67$^+$Pax7$^+$ numbers were reduced markedly in Pα-DTA mice on day 4 after tenotomy (Figures 2J and 2K). Although the frequency of MyoD$^+$ or myogenin$^+$ cells per Pax7$^+$ or M-cad$^+$ cell in Pα-DTA mice was comparable with those in the control (Figures 2K and 2L), suggesting that loss of Pα$^+$ cells did not influence myogenic differentiation of overloaded MuSCs.

Next we investigated the effect of Pα$^+$ cell ablation 11–12 weeks after synergistic ablation (SA), at a late stage of muscle hypertrophy. Although the relative increases in PLA muscle weight and myofiber size in Pα-DTA mice 2 weeks after tenotomy were comparable with control mice (Figures S2C–S2E), these increases were blunted markedly 11–12 weeks after SA (Figures S2F–S2H). Importantly, blunted myonuclear accretion was confirmed even within this period (Figure S2I). These results suggest that Pα$^+$ cells are essential for efficient muscle hypertrophy, including regulation of MuSC expansion.

Yap1 target gene expression in overloaded mesenchymal progenitors

To elucidate the mechanism by which Pα$^+$ cells affect MuSCs in overloaded muscles, we analyzed the transcriptomes of purified Pα$^+$ cells in sham or overloaded muscles on day 2 after tenotomy (Figure 3A). Volcano plot analyses revealed 904 and 638 upregulated and downregulated genes, respectively, in Pα$^+$ cells from overloaded muscles (Figure 3B). Gene Ontology (GO) analyses suggested activation of Pα$^+$ cells because cell cycle-related gene sets were upregulated in overloaded Pα$^+$ cells (Figure S3A). To further investigate the cell cycle-related gene signature in overloaded Pα$^+$ cells, gene set enrichment analyses (GSEA) were performed using oncogenic signature gene sets from the Molecular Signature Database (https://www.gsea-msigdb.org/gsea/). The gene set "CORDENONSI YAP CONSERVED SIGNATURE" was ranked as the top gene signature in this analysis (Figures 3C and 3D), as evidenced by upregulation of many prototypic Yap1 target genes in the overloaded Pα$^+$ cells (Figure 3E), including *Ctgf*. Consistent with this finding, we observed nuclear localized Yap1, which is associated with transcriptional activity, in Pα$^+$ cells located at the distal half of the PLA muscle on days 1 and 2 after tenotomy (Figures 3F and 3G). Nuclear localized Yap1 appeared to be linked to increased mechanical load because Yap1 was rarely observed in nuclei of corresponding regions in sham-operated PLA muscle (Figures 3F and 3G). These results suggest that increased mechanical load leads to activation of Yap1 and induction of its downstream targets in Pα$^+$ cells.

Yap1/Taz in mesenchymal progenitors are critical for MuSC proliferation in overloaded muscles

To elucidate the relevance of Yap1 in Pα$^+$ cells for MuSCs, we generated Pα$^+$ cell-specific Yap1 conditional knockout (cKO) (Y-cKO; *Pdgfra*$^{CreERT/+}$*::Yap1*$^{flox/flox}$) mice and induced overload in PLA muscle by tenotomy (Figure 4A). We also generated Taz cKO (T-cKO; *Pdgfra*$^{CreERT/+}$*::Taz*$^{flox/flox}$) and Yap1/Taz double cKO (cdKO; *Pdgfra*$^{CreERT/+}$*::Yap1*$^{flox/flox}$*::Taz*$^{flox/flox}$) mice, given the known ability of Yap1 and Taz to compensate for each other's loss (Figure 4A). In contrast to Pα-DTA mice (Uezumi et al., 2021), cdKO mice did not show reduced body weight, muscle weight, or myofiber size in sham muscles (Figure 4B). Seven days after tenotomy, no increase in Pα$^+$ cells occurred in cdKO mice, indicating that Yap1/Taz is necessary for the moderate increase in Pα$^+$ cells (Figure 4C). The number of EdU-labeled new myonuclei was significantly lower in cdKO than in control (Cont) mice (*Pdgfra*$^{CreERT/+}$ *or Yap1*$^{flox/flox}$*::Taz*$^{flox/flox}$) (Figure 4D). In contrast, no significant differences were scored in Y-cKO and T-cKO mice, although both strains had a minor reduction in EdU$^+$ myonuclei (Figure 4D). These data suggest partially redundant functions of Yap1 and Taz in overloaded Pα$^+$ cells.

To investigate the influence of Yap1/Taz in overloaded Pα$^+$ cells on MuSC behavior, M-cad$^+$ and EdU$^+$M-cad$^+$ cells were counted in sham and overloaded muscles of Cont and cdKO mice. The results indicated a blunted response to overload in cdKO MuSCs compared with Cont MuSCs (Figures 4E and 4F). Next we investigated the effect of Yap1/Taz loss in overloaded Pα$^+$ cells on MuSC activation. In contrast to Pα-DTA mice, Ki67 expression in Pax7$^+$ cells was not changed significantly in Cont, cdKO, or Y-cKO mice, whereas expansion of

Figure 2. Depletion of mesenchymal progenitor cells reduces the number of MuSC-derived myonuclei in overloaded muscles

(A) Experimental scheme for analyzing control (Cont) and Pα-DTA mice on day 7 after tenotomy.

(B) Ratio of PLA muscle weight (mg) per body weight (g) (left graph) or ratio of tenotomy (Ope) per Sham PLA muscle weight (right graph) of female Cont (n = 4) or Pα-DTA mice (n = 4).

(C) Total myonuclei number per myofiber in Sham and Ope muscles of Cont (n = 5; 1 M, 4 F) and Pα-DTA (n = 6; 2 M, 4 F) mice.

(D) Immunostaining of dystrophin (Dys; green) and EdU in Sham and Ope muscles of Cont and Pα-DTA mice. Arrows or arrowheads indicate myonucleus or non-myonucleus, respectively.

(E) EdU$^+$ myonuclei number in sections from Sham and Ope muscles of Cont (n = 5; 1 M, 4 F) and Pα-DTA (n = 6; 2 M, 4 F) mice.

(F) Immunostaining of M-cadherin (M-cad; red), laminin α2 (green), and EdU in Ope muscles of Cont and Pα-DTA mice. Yellow and white arrowheads indicate M-cad$^+$EdU$^+$ or M-cad$^+$EdU$^-$ cells, respectively.

(G) The number of M-cad$^+$ cells (left) or M-cad$^+$EdU$^+$ cells (right) in sections from Sham and Ope muscles of Cont (n = 5; 1 M, 4 F) and Pα-DTA (n = 5; 2 M, 3 F) mice.

(H) Experimental scheme for analyzing isolated single myofibers from Sham and Ope muscles of Cont and Pα-DTA mice on day 4 (Cont; n = 4; 3 M, 1 F, Pα-DTA ; n = 4; 3 M, 1 F), 7 (Cont; n = 4 M, Pα-DTA; n = 6; 5 M, 1 F), and 10 (Cont; n = 4 F, Pα-DTA ; n = 7; 1 M, 6 F) after tenotomy.

(I) Number of Pax7$^+$ cells on single myofiber from Sham (white bar) and Ope (dot bar) muscles of Cont and Pα-DTA mice at the indicated time point after tenotomy. Pax7$^+$ cell number was calculated by counting 18–30 myofibers per mouse.

(J) Immunostaining of MyoD and Ki67 in Pax7$^+$ cells on freshly isolated myofibers from Ope muscle on day 4 after tenotomy of Cont and Pα-DTA mice.

(K) Frequency of Ki67$^+$ (left) or MyoD$^+$ (right) cells in Pax7$^+$ cells on myofibers from Sham (white bar) and Ope (dot bar) muscles of Cont (n = 4; 3 M, 1 F) and Pα-DTA (n = 4; 3 M, 1 F) mice. Approximately 100 Pax7$^+$ cells were observed per mouse.

(L) Immunostaining of M-cad (red), myogenin (myog; green), and laminin α2 (LNα2; white) in Sham and Ope muscles of Cont and Pα-DTA mice. The graph indicates the frequency of myog$^+$ cells in M-cad$^+$ cells from Cont (n = 4; 1 M, 3 F) and Pα-DTA (n = 5; 2 M, 3 F) mice.

Scale bars, 50 μm (D, F, and J) and 10 μm (L). See also Figure S2.

Please cite this article in press as: Kaneshige et al., Relayed signaling between mesenchymal progenitors and muscle stem cells ensures adaptive stem cell response to increased mechanical load, Cell Stem Cell (2021), https://doi.org/10.1016/j.stem.2021.11.003

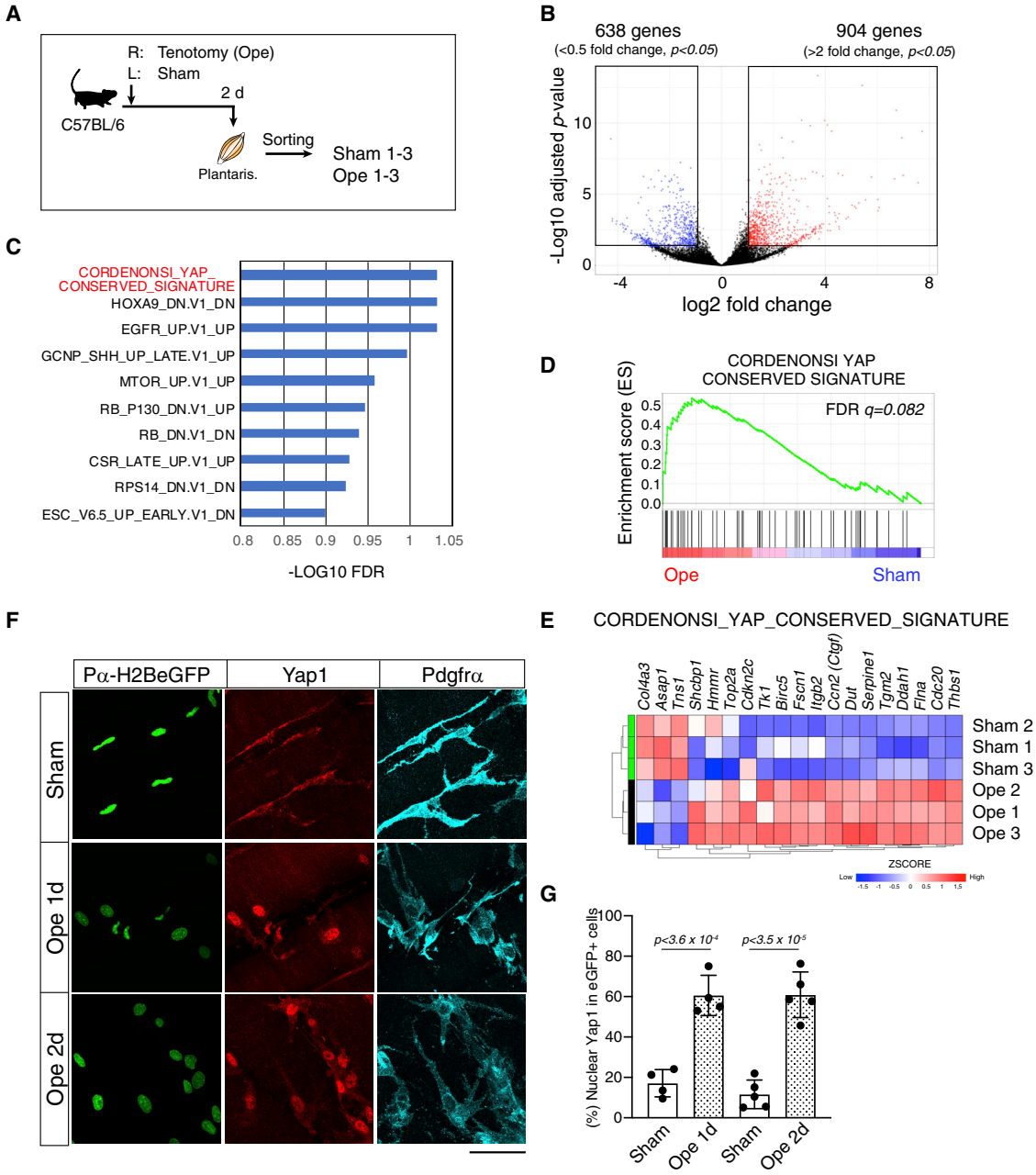

Figure 3. Mechanical overload increases expression of Yap1 target genes in mesenchymal progenitor cells

(A) Experimental scheme for transcriptome analyses in mesenchymal progenitors of Sham and Ope PLA muscle on day 2 after tenotomy in C57BL/6 mice.

(B) The red and blue dots in the volcano plot represent significantly upregulated or downregulated genes, respectively, in mesenchymal progenitors in response to increased mechanical load ($|\log2FC| \geq 1$ and $p < 0.05$).

(C) The top 10 upregulated GSEAs in the mesenchymal progenitors of Ope compared with Sham muscle.

(D) Enrichment plot of "CORDENONSI YAP CONSERVED SIGNATURE" in mesenchymal progenitors from Sham and Ope muscle.

(E) Heatmap of genes involved in Yap1 signature (differently expressed genes in mesenchymal progenitors from Sham (Cont1–Cont3) and Ope (Ope1–Ope3) muscles ($|\log2FC| \geq 1$ and $p < 0.05$) and annotated gene sets in MSigDB).

(F) Whole-mount immunostaining of Yap1, Pdgfrα, and nuclei of Pdgfrα$^+$ cells in Sham and Ope PLA muscle on day 1 and 2 after tenotomy from *Pa-EGFP*. Scale bar, 50 μm.

(G) Percentage of cells with Yap1 accumulation in the nuclei of Pdgfrα$^+$ (EGFP$^+$) cells of Sham and Ope muscles of male *Pa-EGFP* (Ope 1 day, n = 4; Ope 2 day; n = 5).

See also Figure S3.

Please cite this article in press as: Kaneshige et al., Relayed signaling between mesenchymal progenitors and muscle stem cells ensures adaptive stem cell response to increased mechanical load, Cell Stem Cell (2021), https://doi.org/10.1016/j.stem.2021.11.003

CellPress
OPEN ACCESS

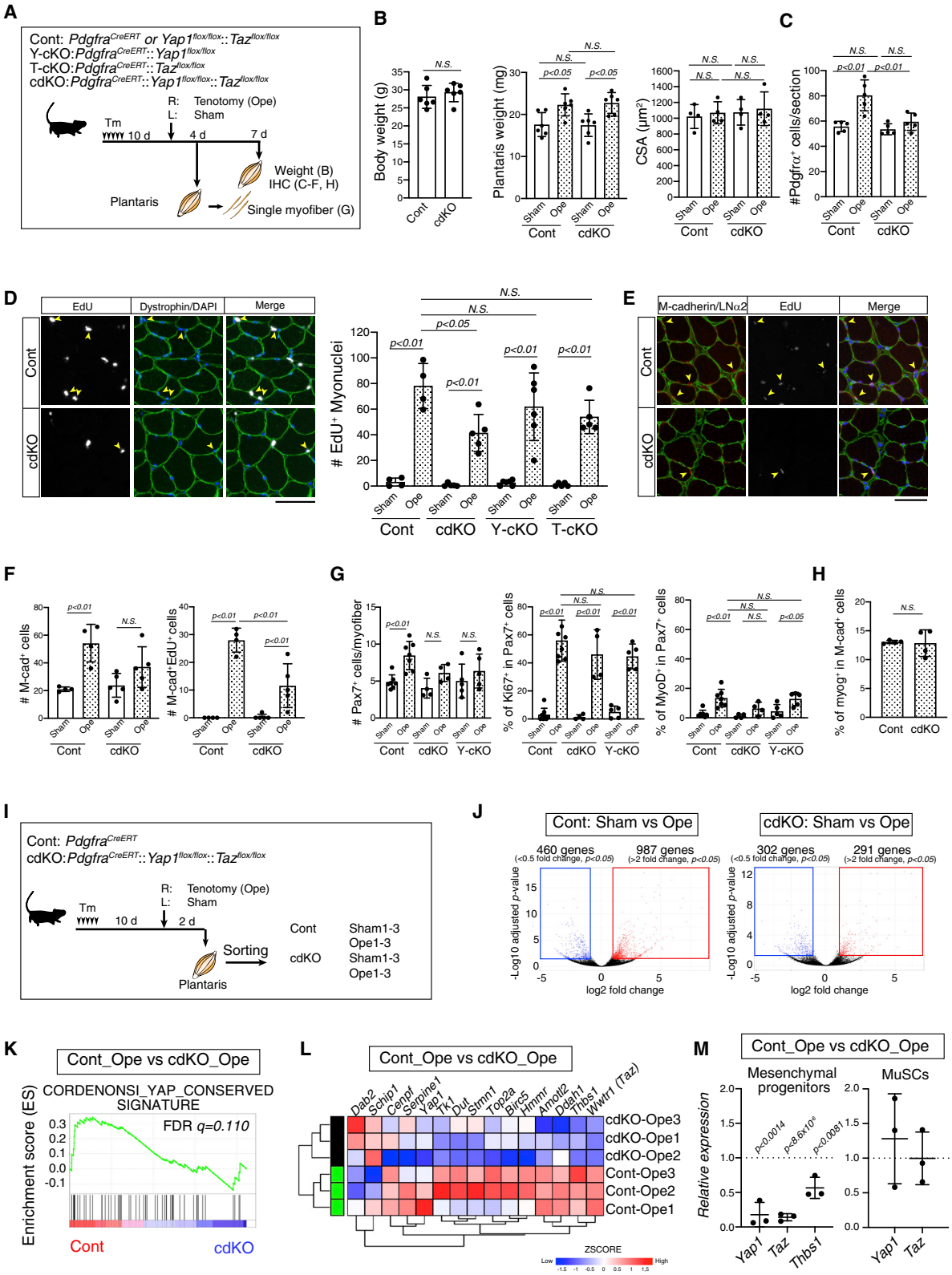

Figure 4. The activity of Yap1 and Taz in mesenchymal progenitor cells is critical for increasing myonuclei in overloaded muscles

(A) Experimental scheme for analyzing Cont, Y-cKO, T-cKO, and, cdKO mice on day 4 and 7 after tenotomy.

(B) Body weight, PLA muscle weight, or myofiber size (CSA) of male Cont (n = 4–6) or cdKO (n = 4–6) mice.

(legend continued on next page)

Pax7$^+$ cells was blunted in cdKO mice (Figure 4G). These results indicate that Yap1/Taz activation in Pα^+ cells is critical for proliferation but not activation of MuSCs in overloaded muscle. Consistent with the results in Pα-DTA mice (Figures 2K and 2L), the frequency of MyoD$^+$ or myogenin$^+$ cells in Pax7$^+$ or M-cad$^+$ cells did not change in cdKO mice (Figures 4G and 4H), suggesting that Yap1/Taz in Pα^+ cells do not govern myogenic differentiation of MuSCs. We also examined the effect of Yap1/Taz loss in muscle hypertrophy 12 weeks after SA and determined that the increase in myofiber size and myonuclear number was blunted in cdKO as well as in Pα-DTA mice (Figures S4A–S4C), indicating that Yap1/Taz in Pα^+ cells are critical for substantial muscle hypertrophy.

To further elucidate the role of Yap1/Taz in Pα^+ cells, RNA sequencing (RNA-seq) analyses of Cont (*Pdgfra*$^{CreERT/+}$*::Yap1*$^{+/+}$*::Taz*$^{+/+}$) and cdKO Pα^+ cells were performed (Figure 4I). The volcano plot analyses indicated that the increase in tenotomy-induced gene expression was attenuated in cdKO Pα^+ cells compared with Cont cells (Figure 4J; 987 versus 291 genes). In addition to the expected decrease in *Yap1* and *Taz* levels, Yap1 target genes were also reduced in cdKO Pα^+ cells compared with Cont from overloaded muscles (Figures 4K–4M). In addition, cell cycle-related GO terms, a signature of loaded Pα^+ cells, were not upregulated in cdKO Pα^+ cells (Figure S3B). These results indicate that increased mechanical load-induced gene expression and activation of Pα^+ cells strongly depend on Yap1/Taz.

Mesenchymal progenitor-derived Thrombospondin-1 promotes muscle stem cell proliferation

Bioinformatics analysis of corresponding ligand-receptor pairs in Pα^+ cells and MuSCs led us to focus on *Thbs1* and *CD47*. *Thbs1*, coding for Thrombospondin-1, was highly expressed in Pα^+ cells in response to overload (Figure S3C), whereas its receptor, CD47, was detected in MuSCs 4 days after tenotomy in quiescent and proliferating MuSCs (Figure S3D). Moreover, *Thbs1* is a Yap1 target gene (Figure 3E), as indicated by reduced expression in Yap1/Taz-deficient Pα^+ cells (Figures 4L and 4M).

We corroborated that expression of *Thbs1* increased specifically in Pα^+ cells 2 days after tenotomy but not in MuSCs and myofibers (Figure 5A). RNA-seq analyses also indicated non-increased expression of *Thbs1* in loaded MuSCs, although other Yap1 target genes were increased (Figure S3E). Furthermore, we determined Thbs1 protein levels in response to overload in muscles and blood by ELISA, which unveiled increased Thbs1 protein concentrations in PLA muscle but not in blood (Figure 5B). Likewise, Pdgfrα^+Thbs1$^+$ cells and Thbs1$^+$ areas were frequently detected in overloaded PLA muscle of wild-type (WT) mice but not in sham and overloaded PLA muscle of Pα-DTA and cdKO mice (Figures 5C, 5D, and S4D–S4F). The analyses of *Thbs1* mRNA expression in the PLA muscle also suggested that Pα^+ cells were the main cell source in loaded muscles because *Thbs1* mRNA was reduced in Pα-DTA and cdKO mice (Figures 5D and S4G). In particular, we noticed that a part of Thbs1 was involved in the basal lamina surrounding myofibers and MuSCs, suggesting that Thbs1 may directly affect MuSC behavior in loaded muscles (Figure 5E). These results indicate that Thbs1 is secreted by Pα^+ cells from overloaded muscles in a Yap1/Taz-dependent manner and acts locally in muscles undergoing hypertrophy.

Thbs1 is a matricellular protein that can interact with a variety of molecules, including the extracellular matrix, cytokines, receptors, and proteases (Resovi et al., 2014). Thbs1-KO mice exhibited some abnormalities, including increased heart weight in males and a decline in muscle weight normalized to body weight in males and females, as reported previously (Figure S5A; Malek and Olfert, 2009). Therefore, to investigate the effect of Thbs1 derived from Pα^+ cells on MuSCs, Pα^+ cells were isolated from WT or Thbs1-KO mice and cultured because nuclear localization of Yap1 and Thbs1 expression are detected in cultured Pα^+ cells (Figure S5B). Importantly, supernatants from Thbs1-KO Pα^+ cells exhibited lower MuSC proliferation on isolated myofibers compared with supernatants from WT Pα^+ cells at 72 h (Figure 5F). Proliferation of Thbs1-KO Pα^+ cells was similar to that of WT Pα^+ cells (Figure S5C). These results strongly indicate that Pα^+ cell-derived Thbs1 accelerates MuSCs proliferation in loaded muscles.

Several integrins (integrins αVβ3, α3β1, α4β1, α6β1, and α9β1), CD36, and CD47 are well-characterized receptors of Thbs1. Because MuSCs express substantial levels of the *Cd47* transcript, but not *Cd36* or the indicated integrins (Figure S3D), and the CD47 agonist PKHB1 (a peptide derived from the Thbs1 C-terminal domain) promoted myoblast proliferation (Figure 5G), we focused on CD47. To examine the importance of

(C) Number of Pdgfrα^+ cells per section from Sham and Ope muscles of Cont (n = 5; 4 M, 1 F) and cdKO mice (n = 5; 4 M, 1 F) on day 7 after tenotomy.
(D) Detection of EdU$^+$ myonuclei (arrowheads) beneath Dys in Ope PLA muscle from Cont and cdKO mice on day 7 after tenotomy. The graph indicates the number of EdU$^+$ myonuclei in Sham and Ope muscles from Cont (n = 4; 3 M, 1 F), Y-cKO (n = 6; 2 M, 4 F), T-cKO (n = 4; 3 M, 1 F), and cdKO (n = 5; 3 M, 2 F) mice.
(E) Immunostaining of M-cad (red), LNα2 (green), and EdU in sections of Ope-7 day muscles from Cont and cdKO mice. Arrowheads indicate M-cad$^+$EdU$^+$ cells.
(F) Number of M-cad$^+$ cells (left) and M-cad$^+$EdU$^+$ cells per section (right) in Sham and Ope muscles from Cont (n = 4; 3 M, 1 F) and cdKO (n = 5; 4 M, 1 F) mice.
(G) Number of Pax7$^+$ cells (left) and frequency of Ki67$^+$ (center) and MyoD$^+$ (right) in Pax7$^+$ cells on single myofibers from Sham and Ope muscles of Cont (n = 7; 6 M, 1 F), Y-cKO (n = 5; 4 M, 1 F), and cdKO (n = 4; 3 M, 1 F) mice. Pax7$^+$ cell number was calculated by counting 16–30 myofibers per mouse.
(H) The frequency of myog$^+$ cells in M-cad$^+$ cells from Ope muscles of Cont (n = 4, 3 M, 1 F) and cdKO (n = 4, 2 M, 2 F) mice.
(I) Experimental scheme for transcriptome analyses of mesenchymal progenitors in Sham and Ope PLA muscle on day 2 after tenotomy of Cont and cdKO mice.
(J) The red and blue dots in the volcano plot represent significantly upregulated and downregulated genes, respectively, in mesenchymal progenitors in response to increased mechanical load ($|\log2FC| \geq 1$ and $p < 0.05$). Left: comparison in Cont mice. Right: comparison in cdKO mice.
(K) Enrichment plot of "CORDENONSI YAP CONSERVED SIGNATURE" in overloaded mesenchymal progenitors of Cont or cdKO mice.
(L) Heatmap of genes involved in Yap1 signature (differently expressed genes in overloaded mesenchymal progenitors) of Cont (Cont; Ope1–Ope3) or cdKO (dKO; Ope1–Ope3) mice ($|\log2FC| > 0.5$ and $p < 0.05$) and annotated gene sets in MSigDB.
(M) Relative gene expression of *Yap1*, *Taz*, and *Thbs1* in overloaded mesenchymal progenitors of cdKO (n = 3) compared with those of Cont mice (n = 3). MuSCs were used for negative Cont for *Yap1* and *Taz* depletion. The y axis indicates the fold change of indicated genes.
Scale bars, 50 μm. See also Figures S3 and S4.

Please cite this article in press as: Kaneshige et al., Relayed signaling between mesenchymal progenitors and muscle stem cells ensures adaptive stem cell response to increased mechanical load, Cell Stem Cell (2021), https://doi.org/10.1016/j.stem.2021.11.003

CellPress
OPEN ACCESS

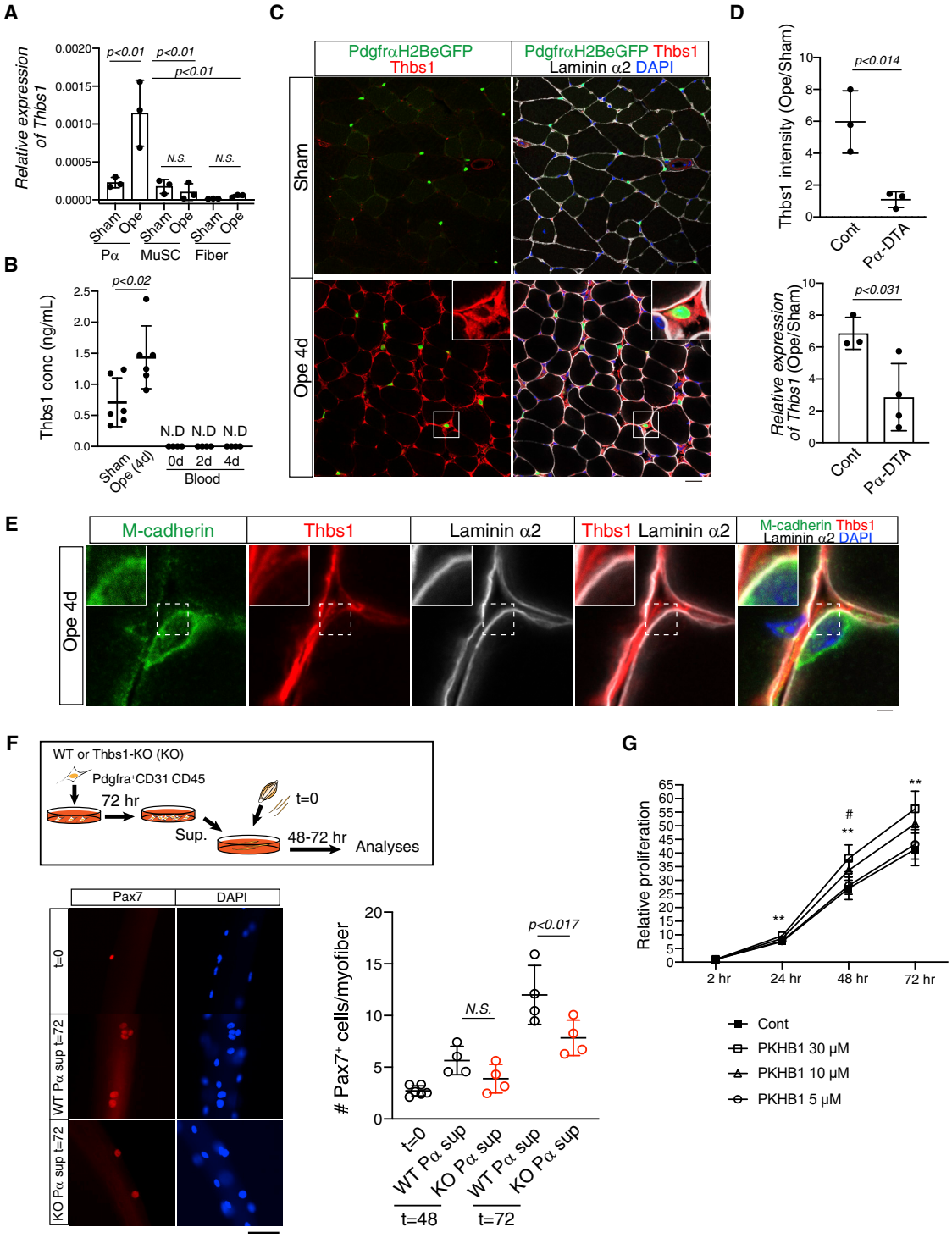

Figure 5. The Thbs1-CD47 axis is indispensable for MuSC proliferation in overloaded muscle

(A) Relative expression of *Thbs1* mRNA in mesenchymal progenitors (Pα^+ cells, n = 3), MuSCs (n = 3), and isolated myofibers (n = 3) from Sham and Ope 2 day muscle of C57BL/6 mice.

(B) Protein concentration of Thbs1 in Sham (n = 6), Ope 4 day (n = 6), and blood (n = 4, each) of C57BL/6 mice on the indicated day after tenotomy.

(C) Immunostaining of Thbs1, LNα2, and nuclei of Pdgfrα^+ cells in sections of Sham and Ope 4 day muscle of *Pa-EGFP*. Scale bar, 25 μm.

(D) The top graph indicates Thbs1$^+$ area in Ope 4 day muscle compared with that in Sham muscle from Cont (n = 3; 2 M, 1 F) or Pα-DTA (n = 3; 1 M, 2 F) mice. The bottom graph indicates *Thbs1* mRNA expression in Ope 4 day muscle compared with that in Sham muscle from Cont (n = 3 F) or Pα-DTA (n = 4 F) mice.

(E) Immunostaining of M-cad, Thbs1, and LNα2 in sections of Ope 4 day muscle. Scale bar, 3 μm.

(legend continued on next page)

CD47 signaling in overloaded muscle, mice were first treated with a monoclonal antibody (mAb) against CD47 (Figure 6A). Intriguingly, the numbers of EdU$^+$ myonuclei were reduced significantly in CD47 mAb-treated mice compared with PBS- or immunoglobulin G (IgG)-treated Cont mice (Figure 6B). In contrast, PKHB1 increased the number of EdU$^+$ new myonuclei in overloaded muscles (Figures 6C and 6D), suggesting that CD47 signaling is critical for MuSC proliferation in overloaded muscle.

To further examine the importance of Thbs1-CD47 signaling in MuSCs, we generated MuSC-specific CD47 cKO mice (CD47-cKO; *Pax7*^{CreERT2}*::Cd47*$^{flox/flox}$) (Figure 6E). As expected, CD47 expression detected in Cont MuSC from sham or loaded muscles was absent in MuSCs from CD47-cKO muscles but not in other cell types, demonstrating efficient cell-type-specific deletion of CD47 (Figures S5D and S5E). CD47-cKO mice revealed a remarkable reduction in EdU-labeled new myonuclei (Figures 6F and 6G), and we observed fewer M-cad$^+$ and M-cad$^+$EdU$^+$ cells in CD47-cKO than in Cont mice (Figures 6H and 6I). Although increased Pax7$^+$ cell numbers were not observed in Cont or CD47-cKO mice 4 days after tenotomy, loss of CD47 in MuSCs did not affect Ki67, MyoD, and myogenin expression (Figures 6J and 6K). The non-increased number of MuSCs likely results from delayed MuSC proliferation in *Pax7*^{CreERT2} mice possessing only one *Pax7* allele. Muscle hypertrophy was blunted 12 weeks after SA but not over 7 days after tenotomy (Figure S6). Further, the effect of PKHB1 disappeared in CD47-cKO mice (Figure 6D), indicating that direct stimulation of CD47 signaling induces MuSC proliferation in loaded muscle. These findings indicate that the Thbs1-CD47 axis is critical for proliferation of MuSCs in overloaded muscle.

The CD47 agonist induces MuSC expansion in CalcR mutant mice

To further corroborate a critical role of CD47 signaling for MuSC expansion, C57BL/6 mice were treated with PKHB1, followed by assessment of MuSC numbers. Interestingly, PKHB1 treatment alone was insufficient to activate quiescent MuSCs and induce their expansion (Figure 7A, 7B, S7A, and S7B), suggesting that additional factors are required for overload-mediated MuSCs proliferation.

Re-analysis of RNA-seq data of overloaded MuSCs (Fukuda et al., 2019) indicated decreased expression of the quiescence-specific genes *Calcr*, *Tenm4*, and *Chrdl2* in MuSCs from overloaded muscles (Figure S3D). We focused our further analysis on CalcR for the following reasons. First, CalcR signaling is an important pathway for maintaining the quiescent state in MuSCs. Although approximately 15%–20% of MuSCs express Ki67, they do not show substantial cell division in Calcr-cKO mice (Yamaguchi et al., 2015). Second, we observed decreased CalcR protein levels in MuSCs from overloaded muscles (Figures 7C and 7D). Moreover, we found an inverse relationship between CalcR and Ki67 expression in MuSCs from overloaded muscles (Figure 7E). Similarly, CalcR expression was retained in Pα-DTA-derived MuSCs without an increase in Ki67 expression, whereas CalcR expression was decreased in cdKO MuSCs showing increased Ki67 expression (Figures 7F and S7C). We therefore investigated whether downregulation of CalcR might enable expansion of MuSCs in response to PKHB1. We treated MuSC-specific CalcR mutant mice (Calcr-cKO) with PKHB1 and counted the number of MuSCs (Figure 7G). Strikingly, PKHB1 administration increased the number of MuSCs in Calcr-cKO mice (Figure 7H) and led to detection of increased numbers of new EdU$^+$ myonuclei and EdU$^+$M-cad$^+$ cells in Calcr-cKO mice (Figures 7I and 7J). These results demonstrate that the coordinated regulation of Thbs1/CD47 and CalcR signaling observed in response to increased mechanical load is sufficient to induce MuSC proliferation.

DISCUSSION

In this study, we demonstrated an essential role of mesenchymal progenitors in regulating MuSC expansion during muscle hypertrophy. We show that increased mechanical load induces transcriptional activation of Yap1/Taz in mesenchymal progenitors, leading to expression of their target genes, including Thbs1. We establish that Thbs1 promotes MuSC proliferation via activation of its receptor CD47 and requires concomitant downregulation of CalcR. Our results identified a Yap1/Taz-Thbs1-CD47 signaling axis that enables mesenchymal progenitors to instruct MuSC expansion during mechanical overload. In addition, our study uncovers a conceptually unexpected paradigm: mesenchymal progenitors respond to mechanical cues and steer MuSC proliferation in overloaded muscle via paracrine Thbs1.

Thbs1 is a large, 150-kDa glycoprotein identified as a major secretory product of thrombin-stimulated platelets. Each domain of Thbs1 interacts with different molecules, resulting in multiple functions, including cell adhesion, motility, proliferation, and survival. The C-terminal domain of Thbs1 is necessary for binding to CD47. We used PKHB1, the first-described serum-stable, soluble CD47-agonist peptide, to activate CD47 in MuSCs, and PKHB1 is a potential therapeutic tool against leukemia (Martinez-Torres et al., 2015). CD47 also functions as a ligand for SIRPα, and blockade of CD47-SIRPα interaction stimulates activation of the immune system, which is considered a potential therapeutic strategy against cancer (Chao et al., 2012). Because infiltration of macrophages, representative SIRPα-expressing cells, is limited in overloaded muscles, our results suggest that Thbs1 is the predominant ligand involved in activation of CD47 signaling in MuSCs. Further studies are required to determine the potential effect of PKHB1 on muscle regeneration by promoting MuSC proliferation in muscular dystrophies.

Consistent with our findings, it has been reported that Thbs1 expression is increased greatly in skeletal muscle following

(F) Experimental scheme for analyzing the effect of Pα^+ cell-derived Thbs1 on Pax7$^+$ cell expansion. Images show Pax7$^+$ cells on freshly isolated myofibers (t = 0) or on myofibers cultured for 72 h with the supernatant of WT or Thbs1-KO Pα^+ cells. The graph indicates the average number of Pax7$^+$ cells on myofibers. Pax7$^+$ cell number was calculated by counting more than 14 myofibers per one mouse. Scale bar, 50 μm.

(G) Effect of PKHB1 on myoblast proliferation. The y axis indicates the relative intensity of luminescence with respect to the beginning (2 h after seeding) of cultivation. **$p < 0.01$, PKHB1 30 μM versus Cont; #$p < 0.05$, PKHB1 10 μM versus Cont.

See also Figures S4 and S5.

Please cite this article in press as: Kaneshige et al., Relayed signaling between mesenchymal progenitors and muscle stem cells ensures adaptive stem cell response to increased mechanical load, Cell Stem Cell (2021), https://doi.org/10.1016/j.stem.2021.11.003

CellPress
OPEN ACCESS

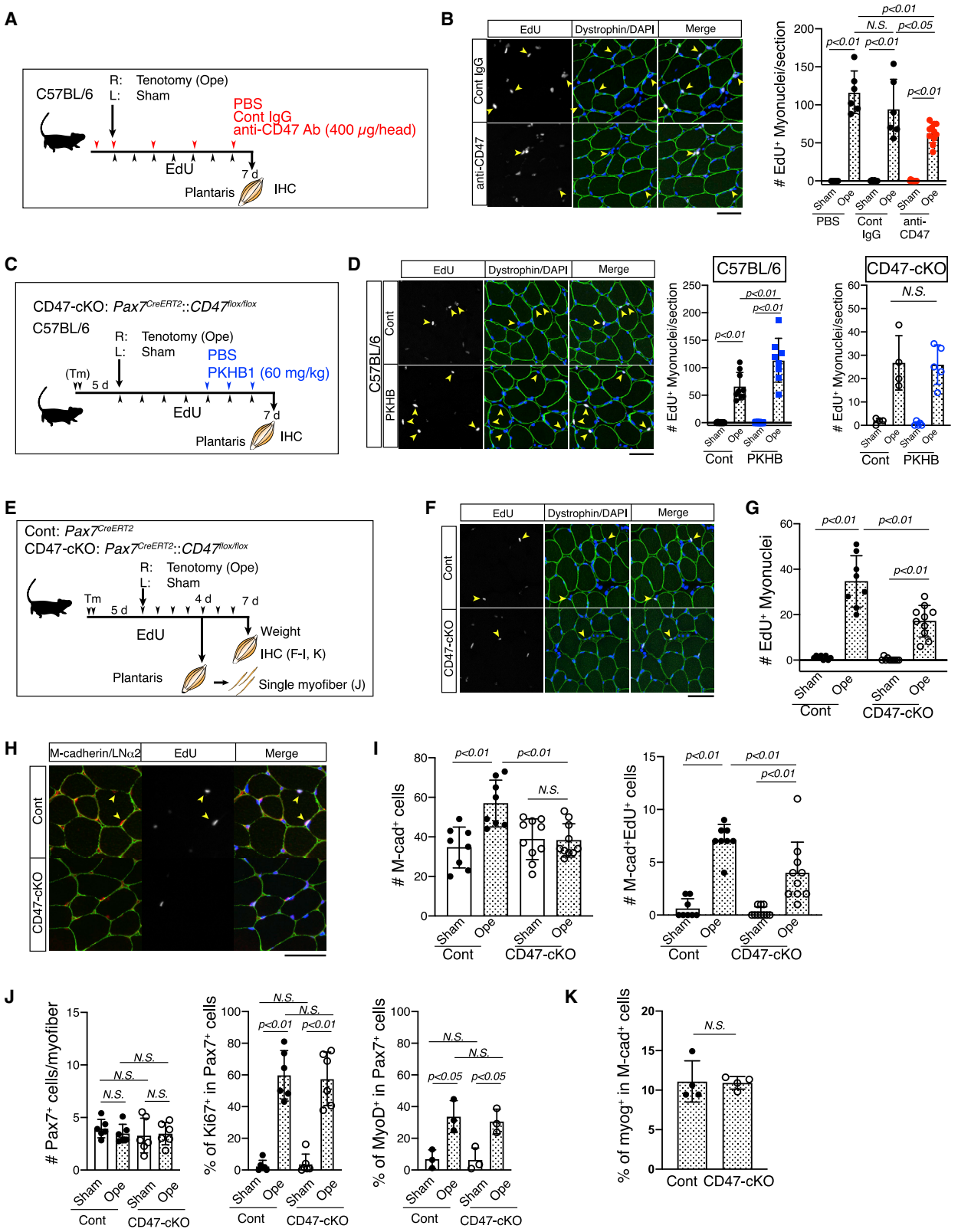

(legend on next page)

active training in mice and humans (Hoier et al., 2013; Olfert et al., 2006). The functions of Thbs1 related to skeletal muscle biology, in particular activation of transforming growth factor β (TGF-β) and anti-angiogenesis, are relatively well investigated. Thbs1 is required for release of TGF-β activation from its latent form, which occurs independent of CD47, and promotes fibrosis in dystrophic muscles (Cohn et al., 2007). In line with this, functional expression of *Col1a1*, a target of TGF-β, increases in mesenchymal progenitors during overload, indicating additional functions of Thbs1 in skeletal muscle hypertrophy. Stimulation of TGF-β activity by Thbs1 also suggests that therapeutic application of Thbs1 needs to done with care to avoid excessive fibrosis. It has been also demonstrated that Thbs1 inhibits cGMP signaling by binding to CD36 and CD47, which suppresses angiogenesis. Increased capillary numbers in Thbs1-null skeletal muscle argue for a physiological role of Thbs1 in inhibition of angiogenesis (Malek and Olfert, 2009). However, the role of Thbs1 upregulation in exercise-triggered angiogenesis is not well understood (Hoier et al., 2013), although induction of angiogenesis by exercise training has been well documented (Olfert et al., 2006). Moreover, the cellular source of Thbs1 remains unidentified. Despite these limitations, our data reveal that mesenchymal progenitors are an important cellular source of Thbs1 and demonstrate an unexpected role of Thbs1 in expansion of MuSCs during muscle hypertrophy.

The signaling processes downstream of CD47 in MuSCs are still unclear. CD47 acts via Gi-cyclic AMP (cAMP) signaling in several cell types (Frazier et al., 1999; Manna and Frazier, 2004; Yao et al., 2011), which corresponds to increased MuSC proliferation and differentiation upon constitutive activation of Gαi2 (Q205L) (Minetti et al., 2014). In our study, however, neither recombinant Thbs1 nor PKHB1 reduced intracellular cAMP levels in forskolin-stimulated C2C12 cells (data not shown). In addition, PKHB1 alone did not induce exit from quiescence, which is secured by CalcR-cAMP-protein kinase A (PKA) signaling in MuSCs (Zhang et al., 2019), suggesting that CD47 signaling in MuSCs does not prevent cAMP accumulation via Gi.

Localization of mesenchymal progenitors within the interstitium can be separated into three regions: endomysium, perimysium, and epimysium. Using single-cell RNA-seq analyses, Muhl et al. (2020) identified Thbs1$^+$Thbs4$^+$Pdgfrα^{low} and Thbs1^{low}Thbs4$^+$ Pdgfrα$^+$ cells in the perimysium and the interface between the perimysium and endomysium, respectively (Muhl et al., 2020). However, the majority of Pdgfrα$^+$ cells in skeletal muscle do not express Thbs1 or Thbs4 or, if at all, then at low levels. Our own RNA-seq analyses in this study indicate that expression of Thbs1 and Thbs4 in mesenchymal progenitors is only low or negative in PLA muscle under baseline conditions but increases dramatically during overload. This finding is in line with immunostaining showing the presence of Thbs1 in the endomysium surrounding myofibers in overloaded muscles. Our results suggest that Pdgfrα$^+$ cells in the endomysium start to express Thbs1 and Thbs4 in response to increased mechanical load.

Pdgfrα is specific to mesenchymal progenitors in skeletal muscle, although Pdgfrα$^+$ cells are present in several other tissues (Uezumi et al., 2010). Hence, ablation of skeletal muscle-resident Pdgfrα$^+$ cells or inactivation of Yap1/Taz were not restricted to skeletal muscle. Thus, we cannot completely exclude an influence of non-muscle Pdgfrα$^+$ cells. However, we compared overloaded muscle with contralateral sham muscle in all experiments, confirming that effects on MuSCs depend on the local overload. In addition, the absence of any abnormality in cdKO mice under steady-state conditions and the unaltered levels of Thbs1 protein in the blood suggest that inactivation of Yap1/Taz or ablation of Pdgfrα$^+$ cells in non-muscle tissues do not have a substantial effect on muscle physiology.

The discovery that MuSC can be expanded in non-injured and non-exercised muscles by CD47 signaling when CalcR expression is downregulated has important implications: First, it indicates that MuSC activation and proliferation during muscle hypertrophy do not require myofiber damage. Second, it provides a new approach to expand endogenous MuSCs *in vivo* for therapeutic purposes. Because MuSCs supply nuclei and mitochondria that are affected during aging, artificial expansion of MuSCs may have therapeutic potential for several disorders. Similarly, therapeutic expansion of MuSC might improve the chance of successful gene delivery into MuSCs for treatment of human muscle dystrophies.

Limitations of the study

Yap1/Taz are known mechanosensors that respond to increased mechanical load and induce transcription of their target genes (Dupont et al., 2011). However, in addition to mechanical cues, alternative pathways might also be responsible for nuclear

Figure 6. The Thbs1-CD47 axis is indispensable for MuSC proliferation in overloaded muscle

(A) Experimental scheme for analyzing the effect of anti-CD47 inhibitory antibodies on myonuclear accretion in C57BL/6 mice.

(B) Immunostaining of Dys and EdU in Ope 7 day muscle of C57BL/6 mice injected with Cont IgG or anti-CD47 antibody. The graph indicates the number of EdU$^+$ myonuclei in Sham and Ope muscles in the PBS (n = 6), Cont IgG (n = 6), or anti-CD47 antibody (n = 11) groups.

(C) Experimental scheme for analyzing the effect of CD47 agonist (PKHB1) on myonuclear accretion in C57BL/6 or CD47-cKO mice.

(D) Immunostaining of Dys and EdU in Ope 7 day muscle of C57BL/6 mice injected with PBS (Cont) or PKHB1. The graphs indicate the number of EdU$^+$ myonuclei in Sham and Ope muscles in Cont and PKHB1 groups of C57BL/6 (left; Cont, n = 9; PKHB1, n = 8) or CD47-cKO (right; Cont, n = 4, 2 M, 2 F; PKHB1, n = 5, 3 M, 2 F) mice. CD47-cKO mice were treated with tamoxifen 5 days before tenotomy.

(E) Experimental scheme for analyzing the effect of MuSC-specific CD47 depletion on myonuclear accretion in overloaded PLA muscle.

(F) Immunostaining of Dys and EdU in Ope 7 day muscle of Cont and CD47-cKO mice.

(G) The number of EdU$^+$ myonuclei in Sham or Ope muscles from Cont (n = 8; 3 M, 5 F) or CD47-cKO (n = 10; 3 M, 7 F) mice.

(H) Immunostaining of M-cad (red), LNα2 (green) and EdU in Ope 7 day muscle of Cont or CD47-cKO mice.

(I) The number of M-cad$^+$ cells (left) or M-cad$^+$EdU$^+$ cells per section (right) in Sham or Ope muscles of Cont (n = 8; 3 M, 5 F) or CD47-cKO (n = 10; 3 M, 7 F) mice.

(J) Number of Pax7$^+$ cells and frequency of Ki67$^+$ and MyoD$^+$ cells in Pax7$^+$ cells on a single myofiber of Sham or Ope 4 day muscle from Cont (n = 6; 3 M, 3 F for Pax7$^+$ and Ki67$^+$; n = 3; 1 M, 2 F for MyoD$^+$) and CD47-cKO (n = 6; 2 M, 4 F for Pax7$^+$ and Ki67$^+$, n = 3; 2 M, 1 F for MyoD$^+$) mice. Pax7$^+$ cell number and frequency were calculated by counting 14–30 myofibers per mouse.

(K) The frequency of myog$^+$ cells in M-cad$^+$ cells from Ope muscles of Cont (n = 4; 3 M, 1 F) and CD47-cKO (n = 4; 3 M, 1 F) mice.

Arrowheads indicate EdU$^+$ myonuclei or M-cad$^+$ cells. Scale bar, 50 μm. See also Figures S5 and S6.

Please cite this article in press as: Kaneshige et al., Relayed signaling between mesenchymal progenitors and muscle stem cells ensures adaptive stem cell response to increased mechanical load, Cell Stem Cell (2021), https://doi.org/10.1016/j.stem.2021.11.003

CellPress
OPEN ACCESS

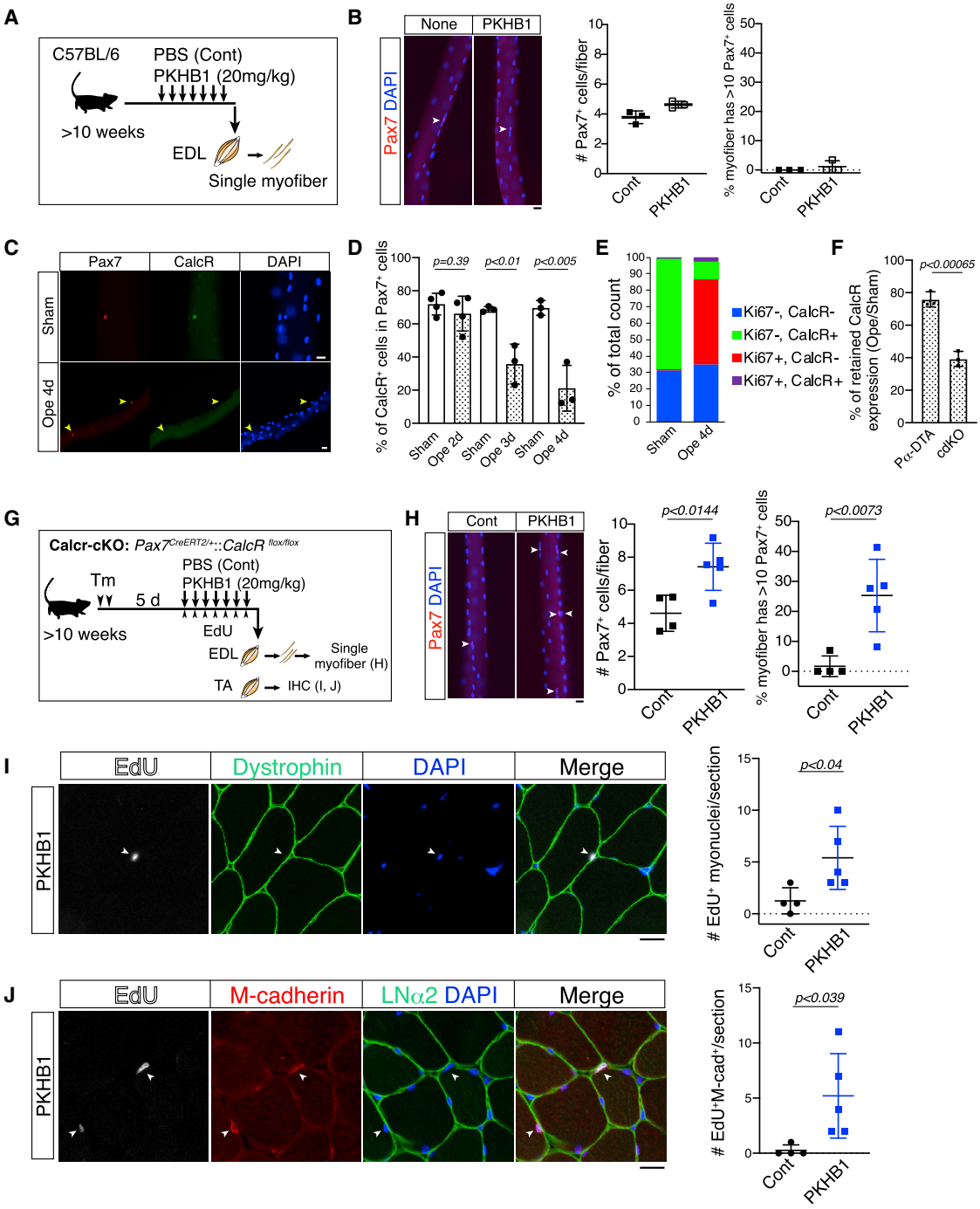

Figure 7. Treatment with a CD47 agonist increases MuSC numbers in CalcR-deficient mice

(A) Experimental scheme for analyzing MuSCs in C57BL/6 mice injected with PBS (Cont) or PKHB1.

(B) Detection of Pax7$^+$ cells (arrowheads) on freshly isolated myofibers. The graph indicates the average number of Pax7$^+$ cells on a single myofiber (left) and the frequency of myofibers harboring more than 10 Pax7$^+$ cells (right) from Cont (n = 3) and PKHB1-treated (n = 3) mice. Pax7$^+$ cell number was calculated by counting 29 myofibers per mouse.

(C) Immunostaining of Pax7 and CalcR in MuSCs on myofibers of Sham or Ope 4 day mice. Arrowheads indicate Pax7$^+$CalcR$^-$ cells.

(D) Frequency of Pax7$^+$CalcR$^+$ cells in Sham and Ope muscle on days 2 (n = 4), 3 (n = 3), and 4 (n = 3) after tenotomy. More than 20 MuSCs were observed per mouse.

(E) Association between CalcR and Ki67 expression in MuSCs from Sham and Ope 4 day muscles. Data indicate the average of two independent experiments. More than 50 MuSCs were observed per mouse.

(F) Graph indicating CalcR expression in Ope 4 day muscle compared with that in Sham muscle from Pα-DTA (n = 3; 2 M, 1 F) or Pα-Yap1/Taz-cdKO (n = 3 M) mice.

(G) Experimental scheme for analyzing MuSCs in Calcr-cKO mice injected with PBS (Cont) or PKHB1.

(legend continued on next page)

translocation of Yap1/Taz. It seems possible that mechanical forces lead to release of growth factors retained in the extracellular matrix, which then induce Yap1/Taz activation. In fact, mechanical overload-dependent release of hepatocyte growth factor (HGF) from the extracellular matrix has been reported (Tatsumi, 2010). Another possibility is that myofibers activate mesenchymal progenitors in response to overload; Reddy et al. (2020) demonstrated that myofiber-secreted succinate acts on mesenchymal progenitors upon exercise (Reddy et al., 2020). Considering the early nuclear translocation of Yap1 in overloaded mesenchymal progenitors, mechanical cue-dependent Yap1/Taz activation seems to be the most likely mechanism for mesenchymal progenitor-mediated MuSC proliferation in overloaded muscle. However, the lack of appropriate tools has limited our ability to prove that mechanical cues directly activate Yap1/Taz in mesenchymal progenitor cells *in vivo*.

Increasing evidence suggests that biological sex has an important effect on several biological processes, including regulation of muscle stem cells. Although we did not find obvious differences among different biological sexes, our study lacks the statistical power to make conclusive statements regarding potential effects of biological sex on the mesenchymal progenitor-Thbs1-CD47 axis in loaded muscles.

STAR★METHODS

Detailed methods are provided in the online version of this paper and include the following:

- KEY RESOURCES TABLE
- RESOURCE AVAILABILITY
  - Lead contact
  - Materials availability
  - Data and code availability
- EXPERIMENTAL MODEL AND SUBJECT DETAILS
  - Mice
  - Muscle overload model
- METHOD DETAILS
  - Muscle fixation and histological analysis
  - Whole-mount immunofluorescence staining
  - *In vivo* EdU labeling and detection
  - Anti-CD47 antibody or PKHB1 administration
  - Measurement of Thbs1
  - Single myofiber isolation and staining
  - Isolation of muscle-derived mononuclear cell
  - RNA-seq and analyses
  - RT-PCR analysis
  - Proliferation assay
  - Single myofiber culture with supernatant experiments from mesenchymal progenitors
- QUANTIFICATION AND STATISTICAL ANALYSIS

SUPPLEMENTAL INFORMATION

Supplemental information can be found online at https://doi.org/10.1016/j.stem.2021.11.003.

ACKNOWLEDGMENTS

This study was supported by a Grant-in-Aid for Scientific Research (B) (to S.-i.F. and A.U.); Challenging Research (Exploratory, 20K21757), an intramural research grant for neurological and psychiatric disorders from NCNP (2-6), the Takeda Science Foundation, the Astellas Foundation for Research on Metabolic Disorders, and Association Française contre les Myopathies (AFM; 23574) (to S.-i.F.); and AMED (JP20am0101084 and JP20am010 1123). Research in the M.P. laboratory was supported by the European Research Council (ERC) Consolidator Grant EMERGE (773047). T.B. was supported by the German Research Foundation (DFG) Transregional Collaborative Research Centre 81 (TP A02), the collaborative research center SFB 1213 (TP B02), and the Transregional Collaborative Research Centre 267 (TP A05). We thank Mitsuo Wada and Kayo Yukawa for constructive discussions regarding our work.

AUTHOR CONTRIBUTIONS

A.K. performed most of the experimental work and wrote the draft of the manuscript. T. Kaji analyzed Yap1/Taz mutant mice. H.S. and A.N. assisted A.K. with certain experiments. L.Z. assisted A.K. to perform blinded experiments. T. Kurosawa and M.I.-U. performed whole-mount immunofluorescence staining. K.T., M.H., Y.S., T.M., M.P., S.W., and T.B. provided critical materials for the study. S.S. and S.-i.F. analyzed RNA-seq data. K.M. and Y.O. performed RNA-seq analyses. A.K., A.U., and S.-i.F. designed experiments and interpreted experimental data. M.P. and T.B. rewrote and edited the manuscript. A.U. and S.-i.F. conceived and supervised the study, mounted figures, and wrote the manuscript. All authors read and approved the final manuscript.

DECLARATION OF INTERESTS

The authors declare no competing interests.

Received: March 18, 2021
Revised: September 24, 2021
Accepted: November 9, 2021
Published: December 1, 2021

REFERENCES

Azzolin, L., Panciera, T., Soligo, S., Enzo, E., Bicciato, S., Dupont, S., Bresolin, S., Frasson, C., Basso, G., Guzzardo, V., et al. (2014). YAP/TAZ incorporation in the β-catenin destruction complex orchestrates the Wnt response. Cell *158*, 157–170.

Bamman, M.M., Roberts, B.M., and Adams, G.R. (2018). Molecular Regulation of Exercise-Induced Muscle Fiber Hypertrophy. Cold Spring Harb. Perspect. Med. *8*, a029751.

Chao, M.P., Weissman, I.L., and Majeti, R. (2012). The CD47-SIRPα pathway in cancer immune evasion and potential therapeutic implications. Curr. Opin. Immunol. *24*, 225–232.

(H) Detection of Pax7$^+$ cells (arrowheads) on freshly isolated myofibers. The graph indicates the average number of Pax7$^+$ cells on single myofibers (left) or the frequency of myofibers harboring more than 10 Pax7$^+$ cells (right) from Cont (n = 4; 2 M, 2 F) or PKHB1-treated Calcr-cKO (n = 5; 3 M, 2 F) mice. Pax7$^+$ cell number was calculated by counting 23–29 myofibers per mouse.
(I) Detection of EdU$^+$ myonuclei (arrowheads) beneath Dys in Calcr-cKO mice treated with PKHB1. The graph indicates the number of EdU$^+$ myonuclei in Cont (n = 4; 2 M, 2 F) or PKHB1-treated Calcr-cKO (n = 5; 3 M, 2 F).
(J) Detection of EdU$^+$M-cad$^+$ cells (arrowheads) beneath the basal lamina (LNα2) in Calcr-cKO mice treated with PKHB1. The graph indicates the number of EdU$^+$M-cad$^+$ cells in Cont (n = 4; 2 M, 2 F) or PKHB1-treated Calcr-cKO (n = 5; 3 M, 2 F) mice.
Scale bar, 20 μm. See also Figure S7.

Choi, K., and Ratner, N. (2019). iGEAK: an interactive gene expression analysis kit for seamless workflow using the R/shiny platform. BMC Genomics *20*, 177.

Cohn, R.D., van Erp, C., Habashi, J.P., Soleimani, A.A., Klein, E.C., Lisi, M.T., Gamradt, M., ap Rhys, C.M., Holm, T.M., Loeys, B.L., et al. (2007). Angiotensin II type 1 receptor blockade attenuates TGF-beta-induced failure of muscle regeneration in multiple myopathic states. Nat. Med. *13*, 204–210.

Collins-Hooper, H., Woolley, T.E., Dyson, L., Patel, A., Potter, P., Baker, R.E., Gaffney, E.A., Maini, P.K., Dash, P.R., and Patel, K. (2012). Age-related changes in speed and mechanism of adult skeletal muscle stem cell migration. Stem Cells *30*, 1182–1195.

Damas, F., Libardi, C.A., and Ugrinowitsch, C. (2018). The development of skeletal muscle hypertrophy through resistance training: the role of muscle damage and muscle protein synthesis. Eur. J. Appl. Physiol. *118*, 485–500.

Darr, K.C., and Schultz, E. (1987). Exercise-induced satellite cell activation in growing and mature skeletal muscle. J. Appl. Physiol. *63*, 1816–1821.

Dupont, S., Morsut, L., Aragona, M., Enzo, E., Giulitti, S., Cordenonsi, M., Zanconato, F., Le Digabel, J., Forcato, M., Bicciato, S., et al. (2011). Role of YAP/TAZ in mechanotransduction. Nature *474*, 179–183.

Ebbeling, C.B., and Clarkson, P.M. (1989). Exercise-induced muscle damage and adaptation. Sports Med. *7*, 207–234.

Egner, I.M., Bruusgaard, J.C., and Gundersen, K. (2016). Satellite cell depletion prevents fiber hypertrophy in skeletal muscle. Development *143*, 2898–2906.

Frazier, W.A., Gao, A.G., Dimitry, J., Chung, J., Brown, E.J., Lindberg, F.P., and Linder, M.E. (1999). The thrombospondin receptor integrin-associated protein (CD47) functionally couples to heterotrimeric Gi. J. Biol. Chem. *274*, 8554–8560.

Fry, C.S., Kirby, T.J., Kosmac, K., McCarthy, J.J., and Peterson, C.A. (2017). Myogenic Progenitor Cells Control Extracellular Matrix Production by Fibroblasts during Skeletal Muscle Hypertrophy. Cell Stem Cell *20*, 56–69.

Fukada, S., Higuchi, S., Segawa, M., Koda, K., Yamamoto, Y., Tsujikawa, K., Kohama, Y., Uezumi, A., Imamura, M., Miyagoe-Suzuki, Y., et al. (2004). Purification and cell-surface marker characterization of quiescent satellite cells from murine skeletal muscle by a novel monoclonal antibody. Exp. Cell Res. *296*, 245–255.

Fukada, S., Uezumi, A., Ikemoto, M., Masuda, S., Segawa, M., Tanimura, N., Yamamoto, H., Miyagoe-Suzuki, Y., and Takeda, S. (2007). Molecular signature of quiescent satellite cells in adult skeletal muscle. Stem Cells *25*, 2448–2459.

Fukada, S.I., Akimoto, T., and Sotiropoulos, A. (2020). Role of damage and management in muscle hypertrophy: Different behaviors of muscle stem cells in regeneration and hypertrophy. Biochim. Biophys. Acta Mol. Cell Res. *1867*, 118742.

Fukuda, S., Kaneshige, A., Kaji, T., Noguchi, Y.T., Takemoto, Y., Zhang, L., Tsujikawa, K., Kokubo, H., Uezumi, A., Maehara, K., et al. (2019). Sustained expression of HeyL is critical for the proliferation of muscle stem cells in overloaded muscle. eLife *8*, e48284.

Goh, Q., and Millay, D.P. (2017). Requirement of myomaker-mediated stem cell fusion for skeletal muscle hypertrophy. eLife *6*, e20007.

Goodman, C.A., Dietz, J.M., Jacobs, B.L., McNally, R.M., You, J.S., and Hornberger, T.A. (2015). Yes-Associated Protein is up-regulated by mechanical overload and is sufficient to induce skeletal muscle hypertrophy. FEBS Lett. *589*, 1491–1497.

Guerci, A., Lahoute, C., Hébrard, S., Collard, L., Graindorge, D., Favier, M., Cagnard, N., Batonnet-Pichon, S., Précigout, G., Garcia, L., et al. (2012). Srf-dependent paracrine signals produced by myofibers control satellite cell-mediated skeletal muscle hypertrophy. Cell Metab. *15*, 25–37.

Hashimshony, T., Senderovich, N., Avital, G., Klochendler, A., de Leeuw, Y., Anavy, L., Gennert, D., Li, S., Livak, K.J., Rozenblatt-Rosen, O., et al. (2016). CEL-Seq2: sensitive highly-multiplexed single-cell RNA-Seq. Genome Biol. *17*, 77.

Hoier, B., Passos, M., Bangsbo, J., and Hellsten, Y. (2013). Intense intermittent exercise provides weak stimulus for vascular endothelial growth factor secretion and capillary growth in skeletal muscle. Exp. Physiol. *98*, 585–597.

Ito, N., Ruegg, U.T., Kudo, A., Miyagoe-Suzuki, Y., and Takeda, S. (2013). Activation of calcium signaling through Trpv1 by nNOS and peroxynitrite as a key trigger of skeletal muscle hypertrophy. Nat. Med. *19*, 101–106.

Joe, A.W., Yi, L., Natarajan, A., Le Grand, F., So, L., Wang, J., Rudnicki, M.A., and Rossi, F.M. (2010). Muscle injury activates resident fibro/adipogenic progenitors that facilitate myogenesis. Nat. Cell Biol. *12*, 153–163.

Kim, D., Paggi, J.M., Park, C., Bennett, C., and Salzberg, S.L. (2019). Graph-based genome alignment and genotyping with HISAT2 and HISAT-genotype. Nat. Biotechnol. *37*, 907–915.

Lemos, D.R., Babaeijandaghi, F., Low, M., Chang, C.K., Lee, S.T., Fiore, D., Zhang, R.H., Natarajan, A., Nedospasov, S.A., and Rossi, F.M. (2015). Nilotinib reduces muscle fibrosis in chronic muscle injury by promoting TNF-mediated apoptosis of fibro/adipogenic progenitors. Nat. Med. *21*, 786–794.

Liao, Y., Smyth, G.K., and Shi, W. (2014). featureCounts: an efficient general purpose program for assigning sequence reads to genomic features. Bioinformatics *30*, 923–930.

Liu, X., Pu, Y., Cron, K., Deng, L., Kline, J., Frazier, W.A., Xu, H., Peng, H., Fu, Y.X., and Xu, M.M. (2015). CD47 blockade triggers T cell-mediated destruction of immunogenic tumors. Nat. Med. *21*, 1209–1215.

Malek, M.H., and Olfert, I.M. (2009). Global deletion of thrombospondin-1 increases cardiac and skeletal muscle capillarity and exercise capacity in mice. Exp. Physiol. *94*, 749–760.

Manna, P.P., and Frazier, W.A. (2004). CD47 mediates killing of breast tumor cells via Gi-dependent inhibition of protein kinase A. Cancer Res. *64*, 1026–1036.

Martinez-Torres, A.C., Quiney, C., Attout, T., Boullet, H., Herbi, L., Vela, L., Barbier, S., Chateau, D., Chapiro, E., Nguyen-Khac, F., et al. (2015). CD47 agonist peptides induce programmed cell death in refractory chronic lymphocytic leukemia B cells via PLCγ1 activation: evidence from mice and humans. PLoS Med. *12*, e1001796.

McCarthy, J.J., Mula, J., Miyazaki, M., Erfani, R., Garrison, K., Farooqui, A.B., Srikuea, R., Lawson, B.A., Grimes, B., Keller, C., et al. (2011). Effective fiber hypertrophy in satellite cell-depleted skeletal muscle. Development *138*, 3657–3666.

Minetti, G.C., Feige, J.N., Bombard, F., Heier, A., Morvan, F., Nürnberg, B., Leiss, V., Birnbaumer, L., Glass, D.J., and Fornaro, M. (2014). Gαi2 signaling is required for skeletal muscle growth, regeneration, and satellite cell proliferation and differentiation. Mol. Cell. Biol. *34*, 619–630.

Moriya, N., and Miyazaki, M. (2018). Akt1 deficiency diminishes skeletal muscle hypertrophy by reducing satellite cell proliferation. Am. J. Physiol. Regul. Integr. Comp. Physiol. *314*, R741–R751.

Muhl, L., Genové, G., Leptidis, S., Liu, J., He, L., Mocci, G., Sun, Y., Gustafsson, S., Buyandelger, B., Chivukula, I.V., et al. (2020). Single-cell analysis uncovers fibroblast heterogeneity and criteria for fibroblast and mural cell identification and discrimination. Nat. Commun. *11*, 3953.

Murach, K.A., White, S.H., Wen, Y., Ho, A., Dupont-Versteegden, E.E., McCarthy, J.J., and Peterson, C.A. (2017). Differential requirement for satellite cells during overload-induced muscle hypertrophy in growing versus mature mice. Skelet. Muscle *7*, 14.

Olfert, I.M., Breen, E.C., Gavin, T.P., and Wagner, P.D. (2006). Temporal thrombospondin-1 mRNA response in skeletal muscle exposed to acute and chronic exercise. Growth Factors *24*, 253–259.

Reddy, A., Bozi, L.H.M., Yaghi, O.K., Mills, E.L., Xiao, H., Nicholson, H.E., Paschini, M., Paulo, J.A., Garrity, R., Laznik-Bogoslavski, D., et al. (2020). pH-Gated Succinate Secretion Regulates Muscle Remodeling in Response to Exercise. Cell *183*, 62–75.e17.

Resovi, A., Pinessi, D., Chiorino, G., and Taraboletti, G. (2014). Current understanding of the thrombospondin-1 interactome. Matrix Biol. *37*, 83–91.

Rosenblatt, J.D., Lunt, A.I., Parry, D.J., and Partridge, T.A. (1995). Culturing satellite cells from living single muscle fiber explants. In Vitro Cell. Dev. Biol. Anim. *31*, 773–779.

Saito, Y., Respatika, D., Komori, S., Washio, K., Nishimura, T., Kotani, T., Murata, Y., Okazawa, H., Ohnishi, H., Kaneko, Y., et al. (2017). SIRPα^{+}

dendritic cells regulate homeostasis of fibroblastic reticular cells via TNF receptor ligands in the adult spleen. Proc. Natl. Acad. Sci. USA *114*, E10151–E10160.

Serrano, A.L., Baeza-Raja, B., Perdiguero, E., Jardí, M., and Muñoz-Cánoves, P. (2008). Interleukin-6 is an essential regulator of satellite cell-mediated skeletal muscle hypertrophy. Cell Metab. *7*, 33–44.

Shinin, V., Gayraud-Morel, B., and Tajbakhsh, S. (2009). Template DNA-strand co-segregation and asymmetric cell division in skeletal muscle stem cells. Methods Mol. Biol. *482*, 295–317.

Subramanian, A., Tamayo, P., Mootha, V.K., Mukherjee, S., Ebert, B.L., Gillette, M.A., Paulovich, A., Pomeroy, S.L., Golub, T.R., Lander, E.S., and Mesirov, J.P. (2005). Gene set enrichment analysis: a knowledge-based approach for interpreting genome-wide expression profiles. Proc. Natl. Acad. Sci. USA *102*, 15545–15550.

Tatsumi, R. (2010). Mechano-biology of skeletal muscle hypertrophy and regeneration: possible mechanism of stretch-induced activation of resident myogenic stem cells. Anim. Sci. J. *81*, 11–20.

Tremblay, A.M., Missiaglia, E., Galli, G.G., Hettmer, S., Urcia, R., Carrara, M., Judson, R.N., Thway, K., Nadal, G., Selfe, J.L., et al. (2014). The Hippo transducer YAP1 transforms activated satellite cells and is a potent effector of embryonal rhabdomyosarcoma formation. Cancer Cell *26*, 273–287.

Uezumi, A., Fukada, S., Yamamoto, N., Takeda, S., and Tsuchida, K. (2010). Mesenchymal progenitors distinct from satellite cells contribute to ectopic fat cell formation in skeletal muscle. Nat. Cell Biol. *12*, 143–152.

Uezumi, A., Ito, T., Morikawa, D., Shimizu, N., Yoneda, T., Segawa, M., Yamaguchi, M., Ogawa, R., Matev, M.M., Miyagoe-Suzuki, Y., et al. (2011). Fibrosis and adipogenesis originate from a common mesenchymal progenitor in skeletal muscle. J. Cell Sci. *124*, 3654–3664.

Uezumi, A., Ikemoto-Uezumi, M., Zhou, H., Kurosawa, T., Yoshimoto, Y., Nakatani, M., Hitachi, K., Yamaguchi, H., Wakatsuki, S., Araki, T., et al. (2021). Mesenchymal Bmp3b expression maintains skeletal muscle integrity and decreases in age-related sarcopenia. J. Clin. Invest. *131*, e139617.

Watt, K.I., Turner, B.J., Hagg, A., Zhang, X., Davey, J.R., Qian, H., Beyer, C., Winbanks, C.E., Harvey, K.F., and Gregorevic, P. (2015). The Hippo pathway effector YAP is a critical regulator of skeletal muscle fibre size. Nat. Commun. *6*, 6048.

Wosczyna, M.N., Konishi, C.T., Perez Carbajal, E.E., Wang, T.T., Walsh, R.A., Gan, Q., Wagner, M.W., and Rando, T.A. (2019). Mesenchymal Stromal Cells Are Required for Regeneration and Homeostatic Maintenance of Skeletal Muscle. Cell Rep. *27*, 2029–2035.e5.

Yamaguchi, M., Watanabe, Y., Ohtani, T., Uezumi, A., Mikami, N., Nakamura, M., Sato, T., Ikawa, M., Hoshino, M., Tsuchida, K., et al. (2015). Calcitonin Receptor Signaling Inhibits Muscle Stem Cells from Escaping the Quiescent State and the Niche. Cell Rep. *13*, 302–314.

Yao, M., Roberts, D.D., and Isenberg, J.S. (2011). Thrombospondin-1 inhibition of vascular smooth muscle cell responses occurs via modulation of both cAMP and cGMP. Pharmacol. Res. *63*, 13–22.

Yu, F.X., Zhao, B., and Guan, K.L. (2015). Hippo Pathway in Organ Size Control, Tissue Homeostasis, and Cancer. Cell *163*, 811–828.

Zhang, L., Noguchi, Y.T., Nakayama, H., Kaji, T., Tsujikawa, K., Ikemoto-Uezumi, M., Uezumi, A., Okada, Y., Doi, T., Watanabe, S., et al. (2019). The CalcR-PKA-Yap1 Axis Is Critical for Maintaining Quiescence in Muscle Stem Cells. Cell Rep. *29*, 2154–2163.e5.

Please cite this article in press as: Kaneshige et al., Relayed signaling between mesenchymal progenitors and muscle stem cells ensures adaptive stem cell response to increased mechanical load, Cell Stem Cell (2021), https://doi.org/10.1016/j.stem.2021.11.003

CellPress
OPEN ACCESS

STAR★METHODS

KEY RESOURCES TABLE

REAGENT or RESOURCE	SOURCE	IDENTIFIER
Antibodies		
FITC rat anti-mouse CD31 (clone 390)	BD Biosciences	Cat# 558738; RRID:AB_397097
PE rat anti-mouse CD31 (clone 390)	Thermo Fisher Scientific	A16201, RRID:AB_2534866
FITC rat anti-mouse CD45 (clone 30-F11)	eBioscience	Cat#11-0451-82; RRID:AB_465050
PE rat anti-mouse CD45 (clone 30-F11)	BD Biosciences	Cat# 553081, RRID:AB_394611
PE rat anti-mouse Sca-1 (clone D7)	BD Biosciences	Cat# 553336; RRID:AB_394792
Biotin rat anti-mouse satellite cells (clone SM/C-2.6)	Fukada et al., 2004	N/A
Mouse anti-mouse Integrin alpha7 (3C12)	MBL International	Cat# K0046-3, RRID:AB_592046
Goat Anti-Mouse IgG MicroBeads antibody	Miltenyi Biotec	Cat# 130-048-402, RRID:AB_244361
Anti-PE MicroBeads antibody	Miltenyi Biotec	Cat# 130-048-801, RRID:AB_244373
Rabbit Anti-Dystrophin Polyclonal	Abcam	Cat# AB15277; RRID: AB_301813
Sheep anti-human M-Cadherin/Cadherin-15	R&D	Cat# AF4096; RRID: AB_10641849
Rabbit Thrombospondin-1 (clone D7E5F)	Cell Signaling Technology	Cat# 37879; RRID:AB_2799123
Rat anti-mouse laminin α2 (clone 4H8-2)	Enzo	Cat# ALX-804-190-C100; RRID:AB_2051764
Biotin goat anti-mouse Pdgfr alpha	R&D	Cat# BAF1062; RRID:AB_2162051
Goat anti-mouse Pdgfr alpha	R&D	Cat# AF1062, RRID:AB_2236897
Goat anti-mouse PDGF R alpha Phycoerythrin Affinity Purified PAb	R&D	Cat# RSD-FAB1062P-100
Biotin rat anti-mouse CD47 (clone miap31)	Biolegend	Cat# 127505; RRID:AB_1134125
InVivoMab anti-mouse CD47 (clone miap31)	Bio X Cell	Cat# BE0270, RRID:AB_2687793
InVivoMab rat IgG2a	Bio X Cell	Cat# BE0089, RRID:AB_1107769
Rabbit anti-MyoD	Santa Cruz	Cat# sc-760 RRID:AB_2148870
Rabbit anti-MyoD	Abcam	Cat# ab133627, RRID:AB_2890928
Mouse anti-Myogenin	BD Biosciences	Cat# 556358, RRID:AB_396383
Rat anti-Ki67	Thermo Fisher Scientific	Cat# 14-5698-82 RRID:AB_10854564
Mouse anti-Pax7 (clone Pax7)	DSHB	DSHB
Rabbit anti-rat Calcitonin receptor	Bio-Rad	Cat# AHP635; RRID:AB_2068967
Rabbit YAP (clone D8H1X) XP(R)	Cell Signaling Technology	Cat# 14074S; RRID:AB_2650491
Cy3 AffiniPure Donkey Anti-Goat IgG (H+L) (min X Ck,GP,Hms,Hrs,Hu, Ms,Rb,Rat Sr Prot)	Jackson Immuno Research Laboratories, Inc.	Cat# 705-165-147; RRID: AB_2307351
Alexa Fluor® 488-AffiniPure Donkey Anti-Rabbit IgG (H+L) (min X Bov,Ck,Gt,GP,Sy Hms,Hrs,Hu,Ms,Rat,Shp Sr Prot)	Jackson Immuno Research Laboratories, Inc.	Cat# 711-545-152; RRID: AB_2313584
Cy3 AffiniPure F(ab')$_2$ Fragment Donkey Anti-Mouse IgG (H+L)	Jackson Immuno Research Laboratories, Inc.	Cat# 715-166-150; RRID: AB_2340816
Donkey anti-Rabbit IgG (H+L) Highly Cross-Adsorbed Secondary Antibody, Alexa Fluor 488	Thermo Fisher Scientific	Cat# A21206; RRID:AB_2535792
Donkey anti-Sheep IgG (H+L) Cross-Adsorbed Secondary Antibody, Alexa Fluor 546	Thermo Fisher Scientific	Cat# A21098; RRID:AB_2535752
Donkey anti-Rat IgG (H+L) Cross-Adsorbed Secondary Antibody, DyLight 488	Thermo Fisher Scientific	Cat# SA5-10026; RRID:AB_2556606
Chemicals, peptides, and recombinant proteins		
Tamoxifen	Sigma-Aldrich	Cat# T5648-1G
Sunflower seed oil	Sigma-Aldrich	Cat# S5007
Collagenase Type I	Worthington Biochemical	Cat# LS004197

(*Continued on next page*)

Continued

REAGENT or RESOURCE	SOURCE	IDENTIFIER
Collagenase Type II	Worthington Biochemical	Cat# LS004204
EdU	Thermo Fisher Scientific	Cat# A10044
VECTASHIELD Mounting Medium with DAPI	Vector	Cat# H1200
Trizol LS reagent	Thermo Fisher Scientific	Cat# 10296028
PKHB1 (NH2-kRFYVVMWKk-COOH)	GenScript Biotech	N/A
Streptavidin-Allophycocyanin	BD Biosciences	Cat# 554067; RRID:AB_10050396
Propidium iodide staining solution	BD Biosciences	Cat# 556463, RRID:AB_2869075
Extraction Buffer 5X PTR	Abcam	Cat# ab193970
Extraction Enhancer Buffer 50X	Abcam	Cat# ab193971
DAPI	Dojindo	Cat# 340-07971
SlowFade Gold Antifade Mountant	Thermo Fisher Scientific	Cat# S36936
Critical commercial assays		
Click-iT(TM) EdU Alexa Fluor 647 Imaging Kit	Thermo Fisher Scientific	Cat# C10340
Mouse THBS1 / Thrombospondin-1 ELISA Kit (Sandwich ELISA)	LSBio	Cat# LS-F4336-1
QIAGEN RNeasy Micro Kit	QIAGEN	Cat# 74004
QIAGEN miRNeasy Mini Kit	QIAGEN	Cat# 217004
QuantiTect Reverse Transcription Kit	QIAGEN	Cat# 205313
TB Green® Premix Ex Taq II	Takara	Cat# RR820
Direct-zol RNA MicroPrep (50 Preps) w/ Zymo-Spin ICColumns (Capped) (Product Supplied w/ 50 mL TRI Reag	ZYMO RESEARCH	Cat# ZYR-R2061-1
Pierce BCA Protein Assay Kit	Thermo Fisher Scientific	Cat# 23227
RealTime-Glo(TM) MT Cell Viability Assay	Promega	Cat# G9711
ApopTag Red *In Situ* Apoptosis Detection Kit	Merck	Cat# S7165
MidiMACS Starting Kit	Miltenyi Biotec	Cat# 130-090-329
Deposited data		
RNA-seq data	Fukuda et al., 2019	GEO: GSE135903
RNA-seq data	This paper	GEO: GSE159082
RNA-seq data	This paper	GEO: GSE162827
Experimental models: Organisms/strains		
Mouse: *B6;129-Pax7tm2.1(cre/ERT2)Fan/J*	The Jackson Laboratory	JAX:# 012476; RRID:IMSR_JAX:012476
Mouse: *B6.Cg-Calcrtm1c(KOMP)Sfuk*	Yamaguchi et al., 2015	RRID:IMSR_RBRC09861
Mouse: *B6;129-Gt(ROSA)26Sortm1(DTA)Mrc/J*	The Jackson Laboratory	JAX:# 010527; RRID:IMSR_JAX:010527
Mouse: *Cd47*-floxed	Saito et al., 2017	CDB1078K http://www2.clst.riken.jp/arg/mutant%20mice%20list.html
Mouse: *B6N.Cg-Tg(Pdgfra-cre/ERT)467Dbe/J*	The Jackson Laboratory	JAX:# 018280; RRID:IMSR_JAX:018280
Mouse: *Yap1tm1.1Dupa/J*	The Jackson Laboratory	JAX:# 027929; RRID:IMSR_JAX:027929
Mouse: *Taz-floxed*	Azzolin et al., 2014	N/A
Mouse: *B6.129S4-Pdgfratm11(EGFP)Sor/J*	The Jackson Laboratory	JAX:# 007669; RRID:IMSR_JAX:007669
Mouse: *B6.129X1-Gt(ROSA) 26Sortm1(EYFP)Cos/J*	The Jackson Laboratory	JAX:# 006148; RRID:IMSR_JAX:006148
Mouse: *B6.129S2-Thbs1tm1Hyn/J*	The Jackson Laboratory	Cat# JAX:006141, RRID:IMSR_JAX:006141
Oligonucleotides		
Primers for genotyping, see Table S1	Eurofins	N/A
Primer: *Thbs1* Forward: AACTG TGACCCTGGACTTGC	Eurofins	N/A
Primer: *Thbs1* Reverse: CTGGT AGCCGAAAACAAAGC	Eurofins	N/A

(*Continued on next page*)

Continued

REAGENT or RESOURCE	SOURCE	IDENTIFIER
Primer: *Yap1* Forward: GCCAT GCTTTCGCAACTGAA	Eurofins	N/A
Primer: *Yap1* Reverse: AGTCAT GGCTTGCTCCCATC	Eurofins	N/A
Primer: *Taz/Wwtr1* Forward: CTCCCC ATGGAAACCGAGAC	Eurofins	N/A
Primer: *Taz/Wwtr1* Reverse: GCTCTG CTCCCGTGAATGAT	Eurofins	N/A
Primer: *18S ribosomal RNA* Forward: CAGT AAGTGCGGGTCATAAGC	Eurofins	N/A
Primer: *18S ribosomal RNA* Reverse: AGTTC GACCGTCTTCTCAGC	Eurofins	N/A
Software and algorithms		
FACSDivaTM	BD Biosciences	RRID:SCR_001456
Hybrid Cell count	https://www.keyence.com/ss/products/microscope/bz-x/products-info/quantify.jsp	N/A
Adobe Illustrator	https://www.adobe.com/products/illustrator.html	RRID:SCR_010279
Photoshop CC	https://www.adobe.com/products/photoshop.html	RRID:SCR_014199
Prism 8	https://www.graphpad.com/scientific-software/prism/	RRID:SCR_005375
iGEAK	https://sites.google.com/view/igeak/manual	N/A
GSEA	https://www.broadinstitute.org/gsea/	RRID:SCR_003199
Leica Application Suite X	https://www.leica-microsystems.com/products/microscope-software/p/leica-las-x-ls/	RRID:SCR_013673
featureCounts (v.2.0.1)	https://bioinf.wehi.edu.au/featureCounts/	RRID:SCR_012919
DESeq2 (v.1.26.0)	https://bioconductor.org/packages/release/bioc/html/DESeq2.html	RRID:SCR_015687
HISAT2 (v.2.2.1)	http://ccb.jhu.edu/software/hisat2/index.shtml	RRID:SCR_015530
Other		
BD FACSAria II Flow Cytometer	BD Biosciences	N/A
All-in-one Fluorescence Microscope BZ-X700	Keyence	N/A
Applied Biosystems Step plus qPCR cycler	Thermo Fisher Scientific	N/A
TCS SP8 confocal laser scanning microscope system	Leica	N/A
Illumina HiSeq 1500 system	Illumina	N/A
ShakeMan	bms	N/A

RESOURCE AVAILABILITY

Lead contact

Further information and requests for resources and reagents should be directed to and will be fulfilled by the lead contact, So-ichiro Fukada (fukada@phs.osaka-u.ac.jp).

Materials availability

This study did not generate new unique reagents.

Data and code availability

RNA-sequencing datasets generated during this study are available at Gene Expression Omnibus (GEO), accession number GEO: GSE159082 and GEO: GSE162827.

EXPERIMENTAL MODEL AND SUBJECT DETAILS

Mice

C57BL/6J mice were purchased from Charles River Laboratories (Yokohama, Kanagawa, Japan). *Calcr*-floxed mice were generated as reported previously (Yamaguchi et al., 2015). *Cd47*-floxed mice were generated at the RIKEN Center for Biosystems Dynamics Research, Kobe, Japan) (association no. CDB1078K) (Saito et al., 2017). *Pax7*^{CreERT2} mice (Stock No: 012476), *Pdgfra*^{CreERT} mice (Stock No: 018280), *Pdgfra-H2B-eGFP* (Stock No: 007669), *Yap1*-floxed (Stock No: 027929), *Rosa26*$^{DTA/+}$ mice (Stock No: 010527), Thbs1-knockout (Stock No: 006141), and *Rosa26*$^{EYFP/+}$ mice (Stock No: 006148) were obtained from Jackson Laboratories (Bar Harbor, ME; Farmington, CT; or Sacramento, CA, USA). *Taz*-floxed mice were kindly provided by Stefano Piccolo (Azzolin et al., 2014). Mice carrying *Pax7*^{CreERT2} or *Pdgfra*^{CreERT} were injected intraperitoneally two or five times (24 h apart) with 200–300 μL tamoxifen (20 mg/mL; Sigma-Aldrich, St. Louis, MO, #T5648) dissolved in sunflower seed oil (Sigma-Aldrich #S5007) and 5% ethanol, and the mice were maintained in a controlled environment (temperature, 24 ± 2°C; humidity, 50% ± 10%) under a 12/12-h light/dark cycle. The mice received sterilized standard chow (DC-8; Nihon Clea, Tokyo, Japan) and water *ad libitum*. All procedures used for experimental animals were approved by the Experimental Animal Care and Use Committee of Osaka University (approval number: 25-9-3, 30-15, R02-3) or Tokyo Metropolitan Geriatric Hospital and Institute of Gerontology (approval number: 20003). Male C57BL/6J mice aged 10-15 weeks were used in all *in vivo* experiments and female mice aged 10-15 weeks were used in all *in vitro* experiments. In experiments using mutant mice, approximately equal numbers of age-matched 10-15 weeks old male and female mice were used. Primer pairs for genotyping were listed in Table S1.

Muscle overload model

Mice were anesthetized with isoflurane. Functional overloading of plantaris muscle (PLA) was induced as described previously (Ito et al., 2013). Under anesthesia, a midline incision was made on the hindlimbs, and the distal tendons of both gastrocnemius and soleus muscles were transected (tenotomy) (Fukuda et al., 2019). The plantaris muscles were isolated at the indicated time points. As the muscle weight no longer increased 2–3 weeks after tenotomy, synergistic ablation (SA) was used to induce long-term and intense overloading in the plantaris muscle. The difference between SA and tenotomy is whether or not the distal half of both the gastrocnemius and the soleus were excised (Fukada et al., 2020). The incision was closed using 6-0 nylon suture with a needle (Natusme Seisakusho, Tokyo, Japan). For the sham-operated group, similar incisions were made, but tenotomy or SA were not performed.

METHOD DETAILS

Muscle fixation and histological analysis

Plantaris and tibialis anterior (TA) muscles were isolated, placed on cork using kneaded Tragacanth Gum (Wako Pure Chemicals Industries, Osaka, Japan) and then frozen in liquid nitrogen-cooled isopentane (Wako Pure Chemicals Industries) for 1 min. After placing the muscles on dry ice for 1 h to vaporize the isopentane, the muscles were stored in closed containers at −80°C.

For immunohistochemical analyses, transverse cryosections (6-μm thick) were fixed with 4% paraformaldehyde (PFA) for 10 min. Detailed information on all antibodies used in this study is listed in the Key resources table. The signals were recorded photographically using a BZ-X700 fluorescence microscope (Keyence, Osaka, Japan).

Whole-mount immunofluorescence staining

Plantaris muscles were fixed with 4% PFA for 30 min. After washing with PBS, muscles were blocked with blocking solution consisting of 1% Triton X-100 and 4% BSA in PBS at 4°C overnight, followed by incubation with primary antibodies diluted in blocking solution at 4°C for one day. Then, muscles were incubated with secondary antibodies diluted in blocking solution at 4°C for one day. Stained muscles were counterstained with DAPI (Dojindo, Kumamoto, Japan) and mounted with SlowFade Gold anti-fade reagent (Thermo Fisher Scientific, Waltham, MA). Z stack images were captured using a TCS SP8 confocal laser scanning microscope system (Leica, Heerbrugg, Switzerland) and reconstructed images were displayed by maximum intensity projection using LAS X software (Leica). As nuclear Yap1 was mainly observed in distal half of overloaded plantaris muscle, 3–4 fields/muscle were captured from the distal half of sham or operated plantaris muscles.

In vivo EdU labeling and detection

EdU (5- ethynyl −2′-deoxyuridine; Thermo Fisher, #A10044) was dissolved in sterilized PBS at 2.5 mg/mL and stored at −20°C. The stock EdU solution was diluted with PBS (0.5 mg/mL) and injected intraperitoneally into mice at 5 mg/kg body weight daily until the day before euthanization. EdU^{+} nuclei were detected using Click-iT EdU Cell Proliferation Kit for Imaging, Alexa Fluor 647 dye (Thermo Fisher, #C10340). For all data, peripheral myonuclei were counted.

Anti-CD47 antibody or PKHB1 administration

Anti-CD47 inhibitory and control antibodies were purchased from Bio X Cell (Lebanon, NH, USA). The antibody solution, diluted to 2.0 mg/mL with sterilized PBS (Tesque, Kyoto, Japan), were intraperitoneally injected into C57BL/6 mice (200 μL per head) at one day before tenotomy and every two days from the day of the surgery (total five times) in accordance with a to previous study (Liu et al., 2015). A CD47 agonist, PKHB1, was purchased from GenScript Biotech (Piscataway, NJ, USA). The peptide (20 or 60 mg/kg) was dissolved in sterilized PBS (Nacalai) and injected intraperitoneally into C57BL/6, CD47-cKO, or CalcR-cKO mice.

Measurement of Thbs1

Lysis buffer was prepared by mixing Extraction Buffer 5X PTR (Abcam, Cambridge, UK, ab193970), Extraction Enhancer Buffer 50X (Abcam, ab193971), and sterilized water. After adding the lysis buffer into the tube containing frozen plantaris muscle according to the muscle weight (100 μL/10 mg), the plantaris muscle was rapidly homogenized using TissueRuptor (QIAGEN, Hilden, Germany). Muscle homogenate was incubated on ice for 20 min, followed by centrifugation at 14,000 × g for 20 min. Supernatant was used as muscle sample for further analyses. Blood was collected from the tail vein and treated with heparin, then centrifuged at 14,000 × g for 5 min to prepare plasma sample. Protein concentrations in muscle and plasma samples were approximately 4–8 mg/mL and 55–65 mg/mL, respectively. Thbs1 protein was detected by mouse THBS1/Thrombospondin-1 (Sandwich ELISA) ELISA Kit-LS-F4336-1) (LSBio, Seattle, WA) and Glomax Microplate Reader (Promega, Madison, WI) according to the manufacturer's protocol. Dilution ratios for muscle and plasma were 1:2 and 1:3, respectively.

Single myofiber isolation and staining

Single myofibers were isolated from plantaris and EDL muscles using collagenase type I (Worthington Biochemical, Lakewood, NJ) using a previously described protocol (Rosenblatt et al., 1995). The isolated myofibers were immediately fixed in 2% PFA for 10 min. After washing the myofibers with PBS, they were permeabilized with a solution containing 20 mM HEPES, 300 mM sucrose, 50 mM NaCl, 3 mM $MgCl_2$, and 0.5% Triton X-100. They were washed with PBS and treated with blocking buffer (PBS containing 5% FCS and 0.01% Triton X-100), followed by incubation with primary antibodies overnight at 4°C. The next day, myofibers were washed with PBS and reacted with secondary antibodies (Collins-Hooper et al., 2012; Shinin et al., 2009). The stained myofibers were placed on glass slide, sealed with VECTASHIELD Mounting Medium with DAPI (Vector Laboratories, Burlingame, CA), and then recorded using a BZ-X700 fluorescence microscope (Keyence).

Isolation of muscle-derived mononuclear cell

Sham or overloaded plantaris muscles were digested using 0.2% collagenase type II (Worthington Biochemical). Mononuclear cells derived from plantaris muscles were stained with FITC-conjugated anti-CD31 and anti-CD45, PE-conjugated anti-Sca-1, and biotinylated-SM/C-2.6 antibodies (Fukada et al., 2004) on ice for 30 min. After washing the cells with PBS containing 2% FBS (washing buffer), the cells were incubated with streptavidin-labeled allophycocyanin (BD Biosciences, Franklin Lakes, NJ) on ice for 30 min. After washing the cells with the washing buffer, the cells were resuspended in washing buffer containing 2 mg/mL propidium iodide (BD Biosciences). Cell sorting was performed using a FACS Aria II flow cytometer (BD Immunocytometry Systems, San Jose, CA). SM/C-2.6$^+$Sca-1$^-$CD31$^-$CD45$^-$ and Sca-1$^+$CD31$^-$CD45$^-$ fractions were used as myogenic cells and mesenchymal progenitor fraction, respectively (Fukada et al., 2007; Joe et al., 2010).

For *in vitro* experiments, MuSCs were isolated using the MACS system. Hindlimb muscles of C57BL/6 female mice were digested with 0.2% collagenase type II, and then mononuclear cells were stained with anti-CD31-PE, CD45-PE, Sca1-PE, and Integrin α7. After washing, the cells were reacted with anti-PE MicroBeads, then CD31, CD45, or Sca1-positve cells were removed using MACS Staring Kit (Miltenyi Biotec Inc.). The CD31/CD45/Sca1 negative cells were reacted with anti-mouse IgG MicroBeads, and Integrin α7-positive cells were isolated. For the preparation of cultured mesenchymal progenitors, mononuclear cells were isolated from WT or Thbs1-KO mice and were cultured for 3 days. Mesenchymal progenitors were purified from crude mononuclear cells using anti-CD31-FITC, CD45-FITC, and Pdgfrα-PE, and Pdgfrα$^+$CD31$^-$CD45$^-$ cells were purified by Aria II. The purified cells within three passages were used for their proliferation assay, and their supernatant experiments with myoblasts. DMEM-LG containing 20% FCS, penicillin-streptomycin, and 5 ng/mL bFGF were used for the expansion of both myoblasts and mesenchymal progenitors.

RNA-seq and analyses

The mesenchymal progenitors were isolated from sham or tenotomy plantaris muscles from six C57BL/6, two control (*Pdgfra*$^{CreERT/+}$*::Yap1*$^{+/+}$*::Taz*$^{+/+}$), and two cdKO (*Pdgfra*$^{CreERT/+}$*::Yap1*$^{flox/flox}$*::Taz*$^{flox/flox}$) mice. The same experiment was repeated to prepare three samples for each group. Cells were sorted into tubes containing Trizol-LS reagent (Thermo Fisher Scientific) at 10,000 cells/tube using a cell sorter (Aria II). RNA was isolated by Direct-zol RNA Microprep (Zymo Research, Irvine, CA, USA).

Libraries were constructed according to the CEL-Seq2 protocol (Hashimshony et al., 2016) for each tube separately and sequenced using an Illumina HiSeq 1500 system (Illumina, San Diego, CA, USA). The obtained single-end reads were mapped to the reference genome (GRCm38) using HISAT2 (v.2.2.1) (Kim et al., 2019). Read counts per gene were determined using featureCounts (v.2.0.1) (Liao et al., 2014). For downstream analyses, including GO analysis, differentially expressed gene analysis, volcano plot, and heatmap visualization, the iGEAK tool kit was leveraged (Choi and Ratner, 2019). The GSEA analysis with the Molecular Signature Database (v.7.2) was performed using the GSEA software (v.4.1.0) (Subramanian et al., 2005). Data were deposited

with the accession number GSE159082 and GSE162827. Gene expression data for myogenic cells at day 4 after tenotomy are available under accession number GSE135903 (Fukuda et al., 2019).

RT-PCR analysis

Total RNA was extracted from sorted cells by using Trizol LS and a QIAGEN RNeasy Micro Kit (QIAGEN) according to the manufacturer's instructions and then reverse-transcribed to cDNA by using a QuantiTect Reverse Transcription Kit (QIAGEN). Total RNA of plantaris muscle was extracted using miRNeasy Mini Kit (QIAGEN) after crushing by Shakeman (BMS, Bio medical science). Specific forward and reverse primers used for optimal amplification of the reverse-transcribed cDNAs using real-time PCR were listed in Key resources table.

Proliferation assay

Two thousand myoblasts or mesenchymal progenitors were seeded in 96-well plate and were cultured in DMEM-LG containing 10% FCS, and penicillin-streptomycin. Proliferation assays were performed using Real-time Glo (Promega) and the luminescence were measured by a Glomax Microplate Reader.

Single myofiber culture with supernatant experiments from mesenchymal progenitors

Pdgfrα^{+}CD31^{-}CD45^{-} cells from wild-type or Thbs1-KO mice were cultured on a collagen-coated dish (Iwaki, #4020-010) for 72 h in DMEM-LG containing 10% FCS, and penicillin-streptomycin. Freshly isolated EDL myofibers from female C57BL/6 mice were maintained in a 1:1 mixture of culture supernatant and fresh culture medium (DMEM-LG containing 10% FCS, and penicillin-streptomycin) that was not refreshed during the cultivation. The myofibers were fixed with 2% PFA at 48 and 72 h after the cultivation. Finally, the number of Pax7-positive cells was counted.

QUANTIFICATION AND STATISTICAL ANALYSIS

Values are expressed as means ± SD. Statistical comparison between two groups was performed by two-sided unpaired Student's t test. For comparison of more than two groups, one-way ANOVA and Tukey-Kramer test (excluding Figure 5G) or Dunnett test (Figure 5G) were used. A p value less than 0.05 was considered to be statistically significant.

Cell Stem Cell, Volume *29*

Supplemental Information

Relayed signaling between mesenchymal progenitors and muscle stem cells ensures adaptive stem cell response to increased mechanical load

Akihiro Kaneshige, Takayuki Kaji, Lidan Zhang, Hayato Saito, Ayasa Nakamura, Tamaki Kurosawa, Madoka Ikemoto-Uezumi, Kazutake Tsujikawa, Shigeto Seno, Masatoshi Hori, Yasuyuki Saito, Takashi Matozaki, Kazumitsu Maehara, Yasuyuki Ohkawa, Michael Potente, Shuichi Watanabe, Thomas Braun, Akiyoshi Uezumi, and So-ichiro Fukada

Cell Stem Cell

Supplemental Information

Relayed signaling between mesenchymal progenitors and muscle stem cells ensures adaptive stem cell response to increased mechanical load

Akihiro Kaneshige, Takayuki Kaji, Lidan Zhang, Hayato Saito, Ayasa Nakamura, Tamaki Kurosawa, Madoka Ikemoto-Uezumi, Kazutake Tsujikawa, Shigeto Seno, Masatoshi Hori, Yasuyuki Saito, Takashi Matozaki, Kazumitsu Maehara, Yasuyuki Ohkawa, Michael Potente, Shuichi Watanabe, Thomas Braun, Akiyoshi Uezumi, So-ichiro Fukada

Supplemental Figures

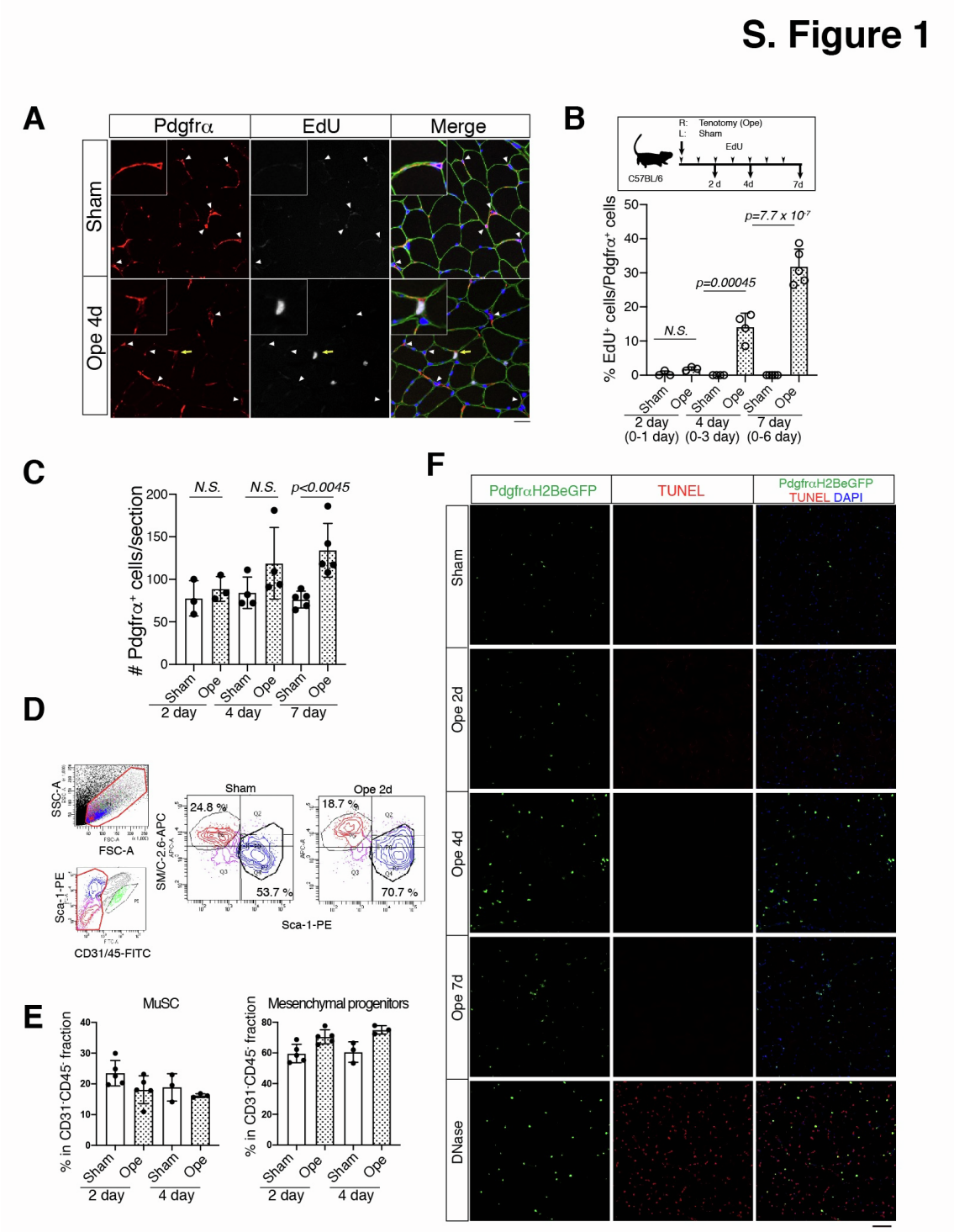

Figure S1. Behaviors of Pα^{+} cells in overloaded muscles; Related to Figure 1

(A) Immunostaining of Pdgfrα (red), laminin α2 (green), and EdU in Sham or Ope muscles on day 4 after tenotomy. Arrows and arrowheads indicate Pdgfrα^{+}EdU^{+} and Pdgfrα^{+}EdU^{-} cells, respectively. Nuclei were counterstained with DAPI. Scale bar: 25 μm

(B) Experimental scheme for analyzing Pdgfrα^{+} cells in plantaris muscle in C57BL/6 mice on day 2, 4, and 7 after tenotomy (Ope; R: right). Contralateral left plantaris muscle was used as sham control (L: Sham). Graph indicates the percentage of EdU^{+} Pdgfrα^{+} cells in Sham and Ope muscles on day 2 (n=3), 4 (n=4), and 7 (n=5) after tenotomy. The number in parentheses refer to the duration of EdU injections.

(C) Number of Pdgfrα^{+} cells per muscle section on day 2, 4, and 7 after tenotomy.

(D) FACS profiles for detecting MuSCs and mesenchymal fractions. The upper left panel shows the gate for the following analyses. The lower left panel shows the gate for CD31^{-}CD45^{-} fraction. The right two panels show MuSCs (SM/C-2.6^{+}Sca-1^{-}) and mesenchymal progenitor fractions (Sca-1^{+}) in CD31^{-}CD45^{-} fraction.

(E) Frequency of MuSC (left) or mesenchymal progenitors (right) in CD31^{-}CD45^{-} fraction in sham or overloaded muscles.

(F) TUNEL staining in sections of Sham and Ope muscles of *PdfgraH2BeGFP* mice on day 2-7 after tenotomy. DNase was used as a positive control of TUNEL staining. Scale bar: 75 μm

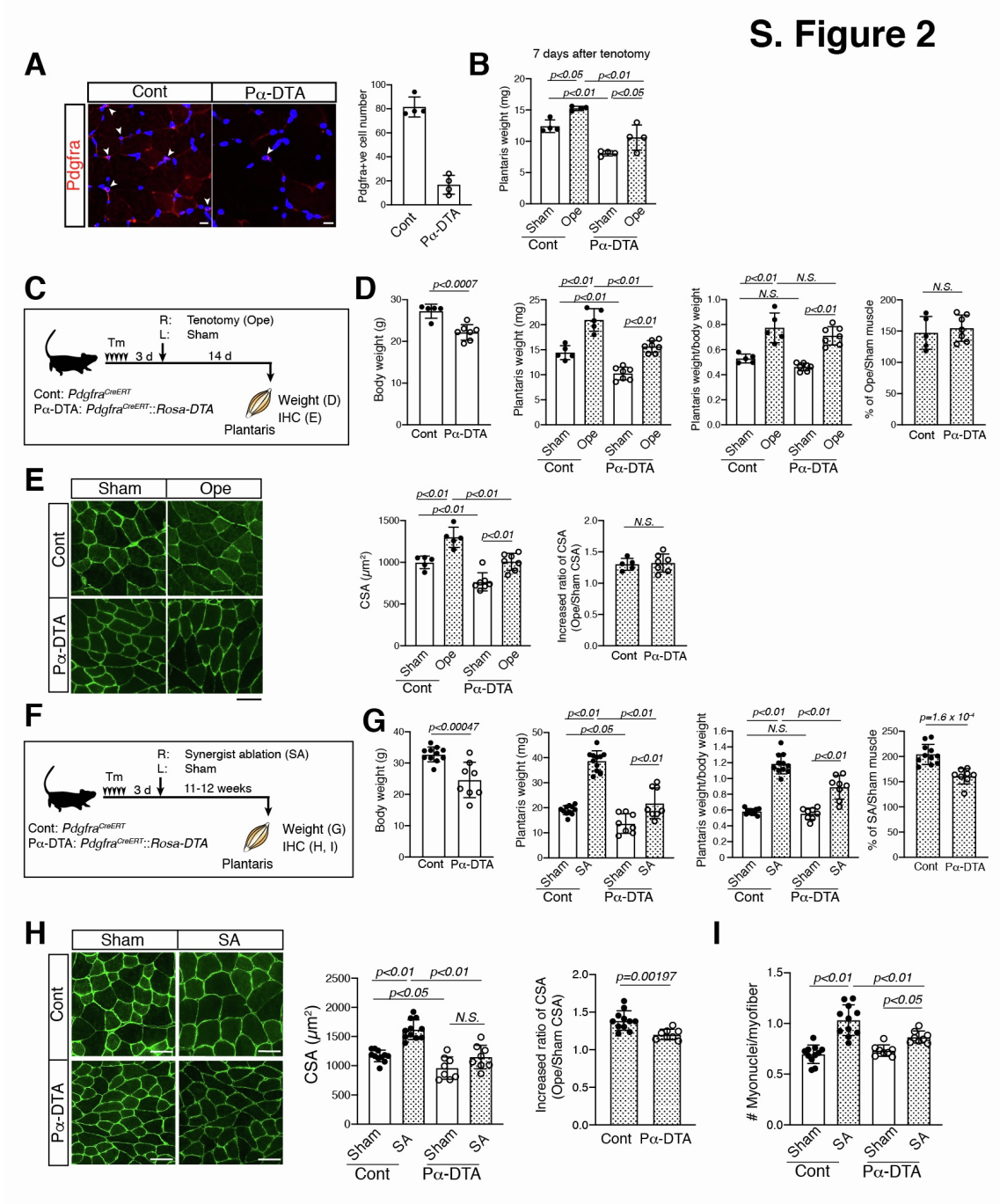

Figure S2. Ablation of Pα cells blunts muscle hypertrophy at 11–12 weeks after synergist ablation (SA); Related to Figure 2

(A) Immunostaining of Pdgfrα (red) in plantaris muscles of Cont and Pα-DTA mice. Arrowheads indicate Pdgfrα^{+} cells. Scale bar: 10 μm. The graph shows the number of

Pdgfrα$^+$ cells per section of plantaris muscles of female Cont (n=4) and Pα-DTA (n=4) mice.

(B) Plantaris muscle weight of sham or overloaded muscle on day 7 after tenotomy of female Cont (n=4) and Pα-DTA (n=4) mice.

(C) Experimental scheme for analyzing the effects of Pα$^+$ cell-depletion on muscle hypertrophy in plantaris muscle two weeks after tenotomy (Ope; R: right). Contralateral left plantaris muscle was used as sham control (L: Sham).

(D) Body weight, plantaris muscle weight, plantaris muscle weight per body weight, or increased ratio of plantaris muscle weight (Ope/Sham) of male control (n=5) or Pα-DTA mice (n=7)

(E) Representative muscle sections stained with anti-laminin α2 (green) antibody for calculating CSA. The graphs show CSA (left) or increased ratio of CSA (Ope/Sham, right) of male control (n=5) or Pα-DTA (n=7) mice. Scale bar: 50 μm

(F) Experimental scheme for analyzing the effects of Pα$^+$ cell-depletion on muscle hypertrophy in plantaris muscle 11–12 weeks after SA (R: SA). Contralateral left plantaris muscle was used as sham control (L: Sham).

(G) Body wight, plantaris muscle weight, plantaris muscle weight per body weight, or increased ratio of plantaris muscle weight (SA/Sham) of male control (n=11) or Pα-DTA (n=8) mice.

(H) Representative muscle sections stained with anti-laminin α2 (green) antibody for calculating CSA. The graphs indicate CSA (left) or increased ratio of CSA (SA/Sham, right) of male control (n=11) mice or Pα-DTA (n=8) mice. Scale bar: 50 μm

(I) Myonuclear number/myofiber in Sham or SA plantaris muscles of male control (n=11) or Pα-DTA (n=8) mice.

S. Figure 3

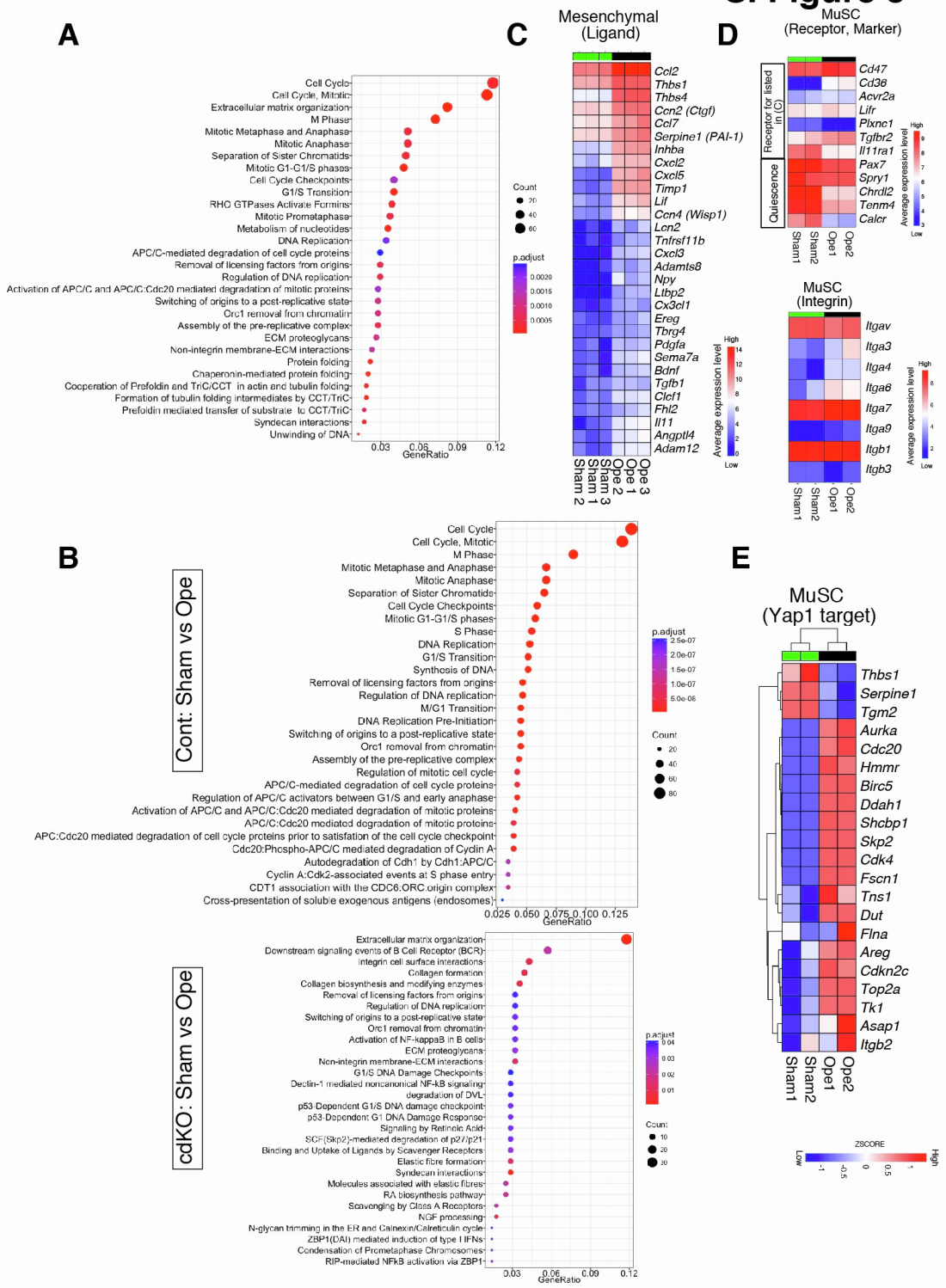
A
Cell Cycle
Cell Cycle, Mitotic
Extracellular matrix organization
M Phase
Mitotic Metaphase and Anaphase
Mitotic Anaphase
Separation of Sister Chromatids
Mitotic G1-G1/S phases
Cell Cycle Checkpoints
G1/S Transition
RHO GTPases Activate Formins
Mitotic Prometaphase
Metabolism of nucleotides
DNA Replication
APC/C-mediated degradation of cell cycle proteins
Removal of licensing factors from origins
Regulation of DNA replication
Activation of APC/C and APC/C:Cdc20 mediated degradation of mitotic proteins
Switching of origins to a post-replicative state
Orc1 removal from chromatin
Assembly of the pre-replicative complex
ECM proteoglycans
Non-integrin membrane-ECM interactions
Protein folding
Chaperonin-mediated protein folding
Cooperation of Prefoldin and TriC/CCT in actin and tubulin folding
Formation of tubulin folding intermediates by CCT/TriC
Prefoldin mediated transfer of substrate to CCT/TriC
Syndecan interactions
Unwinding of DNA
0.03
0.06
0.09
0.12
GeneRatio
Count
20
40
60
p.adjust
0.0020
0.0015
0.0010
0.0005
C
Mesenchymal
(Ligand)
Ccl2
Thbs1
Thbs4
Ccn2 (Ctgf)
Ccl7
Serpine1 (PAI-1)
Inhba
Cxcl2
Cxcl5
Timp1
Lif
Ccn4 (Wisp1)
Lcn2
Tnfrsf11b
Cxcl3
Adamts8
Npy
Ltbp2
Cx3cl1
Ereg
Tbrg4
Pdgfa
Sema7a
Bdnf
Tgfb1
Clcf1
Fhl2
Il11
Angptl4
Adam12
Sham 2
Sham 1
Sham 3
Ope 2
Ope 1
Ope 3
Average expression level
High
Low
D
MuSC
(Receptor, Marker)
Receptor for listed in (C)
Quiescence
Cd47
Cd36
Acvr2a
Lifr
Plxnc1
Tgfbr2
Il11ra1
Pax7
Spry1
Chrdl2
Tenm4
Calcr
Sham1
Sham2
Ope1
Ope2
MuSC
(Integrin)
Itgav
Itga3
Itga4
Itga6
Itga7
Itga9
Itgb1
Itgb3
B
Cont: Sham vs Ope
Cell Cycle
Cell Cycle, Mitotic
M Phase
Mitotic Metaphase and Anaphase
Mitotic Anaphase
Separation of Sister Chromatids
Cell Cycle Checkpoints
Mitotic G1-G1/S phases
S Phase
DNA Replication
G1/S Transition
Synthesis of DNA
Removal of licensing factors from origins
Regulation of DNA replication
M/G1 Transition
DNA Replication Pre-Initiation
Switching of origins to a post-replicative state
Orc1 removal from chromatin
Assembly of the pre-replicative complex
Regulation of mitotic cell cycle
APC/C-mediated degradation of cell cycle proteins
Regulation of APC/C activators between G1/S and early anaphase
Activation of APC/C and APC/C:Cdc20 mediated degradation of mitotic proteins
APC/C:Cdc20 mediated degradation of mitotic proteins
APC:Cdc20 mediated degradation of cell cycle proteins prior to satisfaction of the cell cycle checkpoint
Cdc20:Phospho-APC/C mediated degradation of Cyclin A
Autodegradation of Cdh1 by Cdh1:APC/C
Cyclin A:Cdk2-associated events at S phase entry
CDT1 association with the CDC6:ORC:origin complex
Cross-presentation of soluble exogenous antigens (endosomes)
0.025
0.050
0.075
0.100
0.125
GeneRatio
p.adjust
2.5e-07
2.0e-07
1.5e-07
1.0e-07
5.0e-08
Count
20
40
60
80
cdKO: Sham vs Ope
Extracellular matrix organization
Downstream signaling events of B Cell Receptor (BCR)
Integrin cell surface interactions
Collagen formation
Collagen biosynthesis and modifying enzymes
Removal of licensing factors from origins
Regulation of DNA replication
Switching of origins to a post-replicative state
Orc1 removal from chromatin
Activation of NF-kappaB in B cells
ECM proteoglycans
Non-integrin membrane-ECM interactions
G1/S DNA Damage Checkpoints
Dectin-1 mediated noncanonical NF-kB signaling
degradation of DVL
p53-Dependent G1/S DNA damage checkpoint
p53-Dependent G1 DNA Damage Response
Signaling by Retinoic Acid
SCF(Skp2)-mediated degradation of p27/p21
Binding and Uptake of Ligands by Scavenger Receptors
Elastic fibre formation
Syndecan interactions
Molecules associated with elastic fibres
RA biosynthesis pathway
Scavenging by Class A Receptors
NGF processing
N-glycan trimming in the ER and Calnexin/Calreticulin cycle
ZBP1(DAI) mediated induction of type I IFNs
Condensation of Prometaphase Chromosomes
RIP-mediated NFkB activation via ZBP1
0.03
0.06
0.09
0.12
GeneRatio
p.adjust
0.04
0.03
0.02
0.01
Count
10
20
30
E
MuSC
(Yap1 target)
Thbs1
Serpine1
Tgm2
Aurka
Cdc20
Hmmr
Birc5
Ddah1
Shcbp1
Skp2
Cdk4
Fscn1
Tns1
Dut
Flna
Areg
Cdkn2c
Top2a
Tk1
Asap1
Itgb2
Sham1
Sham2
Ope1
Ope2
ZSCORE
Low
High
-1
-0.5
0
0.5
1

Figure S3. RNA-seq analyses of overloaded mesenchymal progenitors and muscle satellite cells (MuSCs); Related to Figure 3 and 4

(A) Upregulated Biological Process categories (|log2FC| ≥1 and p<0.05) in mesenchymal progenitors from overloaded muscle on day 2 after tenotomy compared to those from sham muscle.

(B) Upregulated Biological Process categories (|log2FC| ≥1 and p<0.05) in mesenchymal progenitors from overloaded muscle of Cont (upper) or cdKO (lower) mice on day 2 after tenotomy compared to those from sham muscle.

(C) Heatmap of genes encoding secreted proteins that were highly expressed (|log2FC| ≥2 and p<0.05) in mesenchymal progenitors from overloaded plantaris muscle. Ope1–3: mesenchymal progenitors derived from overloaded plantaris muscles, Sham1–3: mesenchymal progenitors derived from sham plantaris muscles.

(D) Heatmap of genes encoding receptors related to (C), quiescence genes (*Spry1, Chrdl2, Tenm4, Calcr*), or integrins (*Itga7* and *Itgb1*: positive controls) in MuSCs from overloaded muscle on day 4 after tenotomy (Ope1-2) and sham muscle (Sham1–2). Data deposited with accession number GSE135903 were used in these analyses.

(E) Heatmap of genes involved in Yap1 signature (annotated gene sets in MSigDB) in MuSCs from overloaded muscle on day 4 after tenotomy (Ope1-2) and sham muscle (Sham1–2).

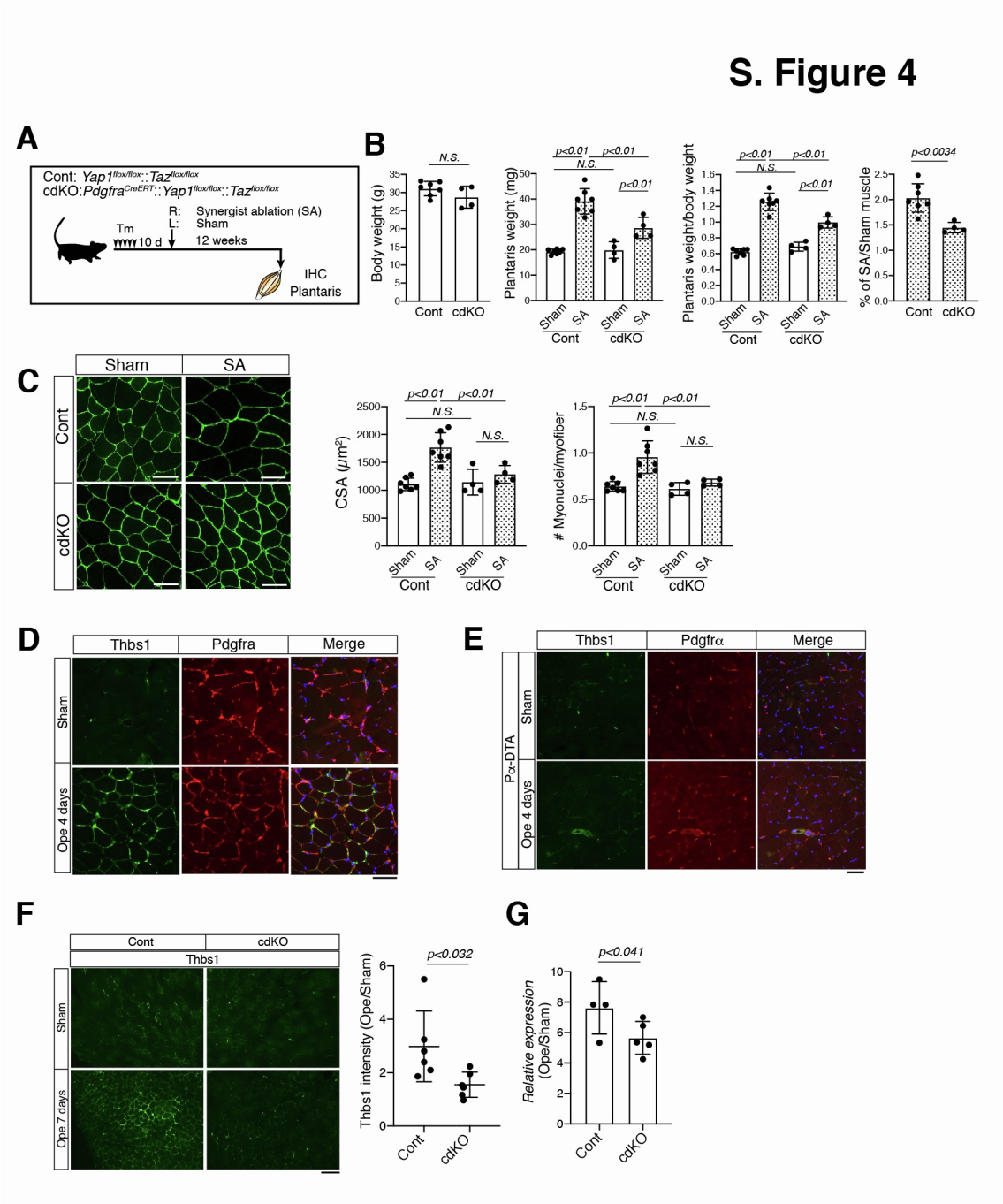

Figure S4. Blunted muscle hypertrophy and reduced expression of Thbs1 in mesenchymal progenitor-specific inactivation of Yap1/Taz; Related to Figure 4 and 5

(A) Experimental scheme for analyzing effects of Pdgfrα-specific Yap1/Taz-depletion on plantaris muscle hypertrophy 12 weeks after SA (R: SA). Contralateral left plantaris muscle was used as sham control (L: Sham).

(B) Body wight, plantaris muscle weight, plantaris muscle weight per body weight, or increased ratio of plantaris muscle weight (SA/Sham) of male control (n=7) or cdKO (n=4) mice.

(C) Representative muscle sections stained with anti-laminin α2 (green) antibody for calculating CSA. The graphs indicate CSA (left) or myonuclear number/myofiber (right) of male control (n=7) or cdKO (n=4) mice. Scale bar: 50 μm

(D) Immunostaining of Pdgfrα (red) and Thbs1 (green) in sections of Sham and overloaded plantaris muscle 4 days after tenotomy (Ope 4d) of control mice (Cont: *Pdgfra*$^{CreERT/+}$). Scale bar: 50 μm

(E) Immunostaining of Pdgfrα (red) and Thbs1 (green) in sections of sham or overloaded plantaris muscles in Pα-DTA mice on day 4 after tenotomy (Ope 4d). Nuclei were counterstained with DAPI. Scale bar: 50 μm

(F) Immunostaining of Thbs1 (green) in sections of sham and overloaded plantaris muscle 7 days after tenotomy (Ope 7d) from control (Cont, *Pdgfra*^{CreERT}) and cdKO mice. Scale bar: 100 μm. The graph indicates Thbs1^{+} area in sham per Ope 7d muscle of Cont (n=6; five male and one female) and cdKO (n=6; four male and two female) mice.

(G) The graph indicates *Thbs1* mRNA expression in Ope 4d muscle per that in Sham muscle from Cont (n=4; two male and two female) or cdKO (n=5; two male and three female).

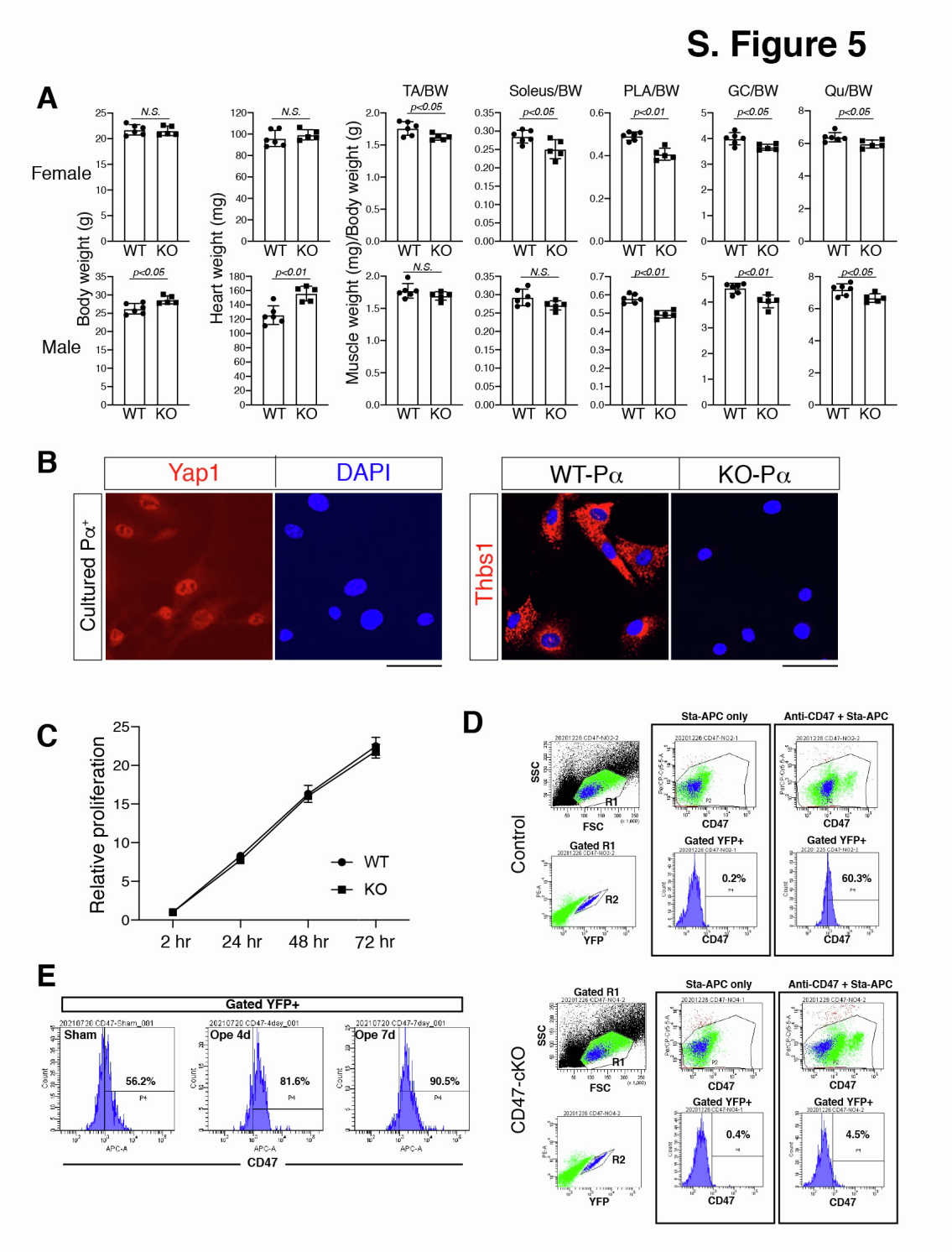

Figure S5. Validation of Thbs1-KO Pα^{+} cells proliferation and expression of CD47 in MuSCs; Related to Figure 5 and 6

(A) Body weight, heart weight or normalized muscle weight of Thbs1-KO mice.

(B) Immunostaining of Yap1 (left) or Thbs1 (right) in cultured Pdfgrα^{+} cells from WT or Thbs1-KO. Nuclei were counterstained with DAPI. Scale bar: 50 μm

(C) Proliferation of mesenchymal progenitors *in vitro*. The Y-axis indicates the relative intensity of luminescence with respect to the beginning (2 hours after seeding) of the cultivation.

(D) CD47 expression in MuSCs of control (*Pax7*^{CreERT2}*::Cd47*$^{+/+}$*::Rosa-YFP*) (upper) or CD47-cKO (*Pax7*^{CreERT2}*::Cd47*$^{flox/flox}$*::Rosa-YFP*) mice (lower). CD47 expression was detected in control MuSC fraction gated R1 (FCS/SSC plot) & R2 (YFP^{+} fraction), but not in CD47-cKO MuSCs. Other CD47^{+} cells (green dots) were detected in both control and CD47-cKO MuSCs, indicating MuSC-specific deletion of CD47 in CD47-cKO mice. Blue dots show MuSC fraction in all panels.

(E) The histograms show CD47 expression in MuSCs from Sham or loaded plantaris muscle 4 or 7 days after tenotomy of control (*Pax7*^{CreERT2}*::Cd47*$^{+/+}$*::Rosa-YFP*) mice.

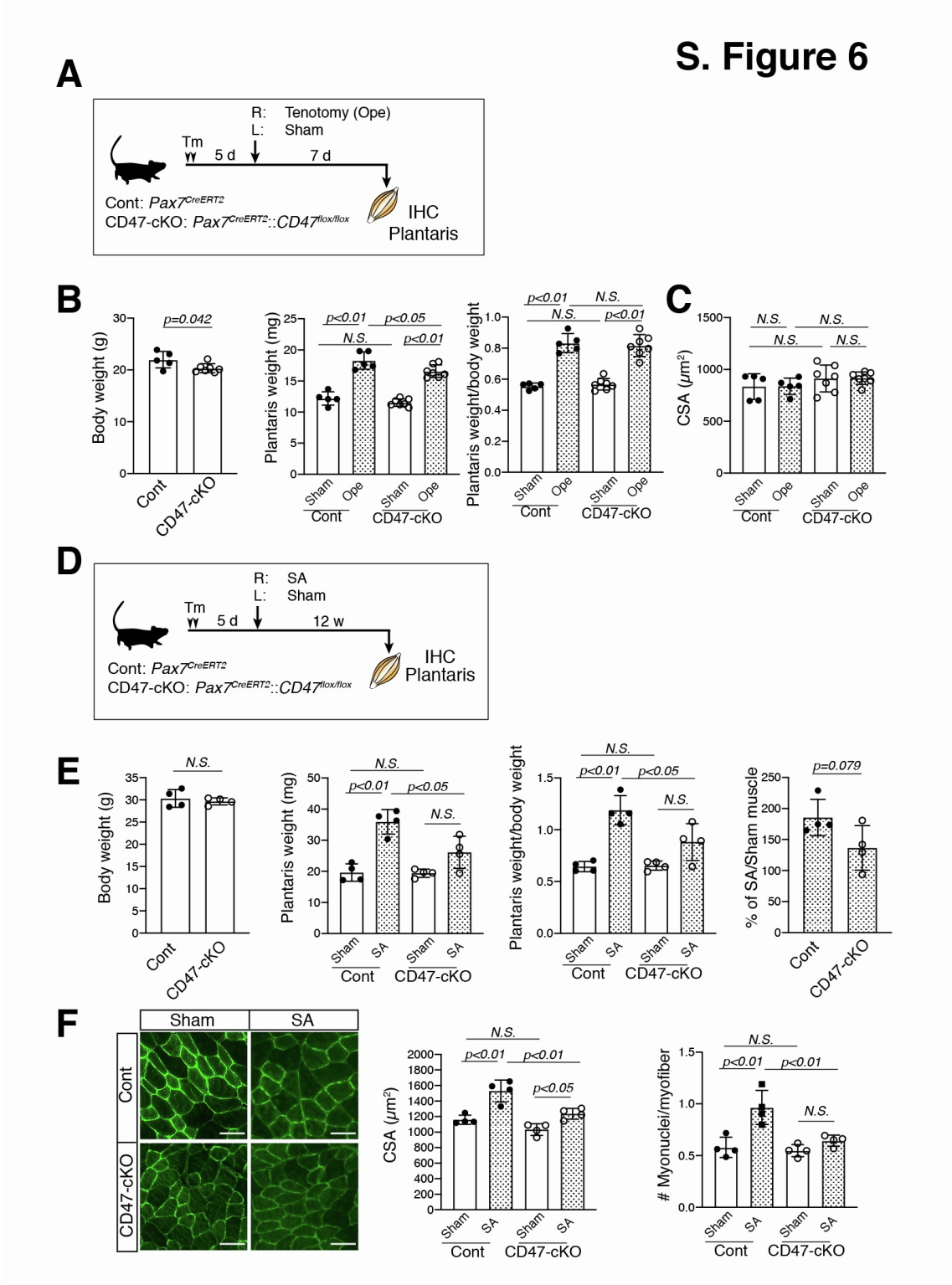

Figure S6. Loss of CD47 in MuSC blunts muscle hypertrophy at 12 weeks after synergist ablation (SA); Related to Figure 6

(A) Experimental scheme for analyzing effects of MuSC specific CD47-depletion on

plantaris muscle hypertrophy 7 days after tenotomy (R: Ope). Contralateral left plantaris muscle was used as sham control (L: Sham).

(B) Body weight (left), plantaris muscle weight (middle), or plantaris muscle weight per body weight (right) of female control (n=5) or CD47-cKO (n=7) mice.

(C) Myofiber size (CSA: cross sectional area) of female control (n=5) or CD47-cKO (n=7) mice.

(D) Experimental scheme for analyzing effects of MuSC specific CD47-depletion on plantaris muscle hypertrophy 12 weeks after SA (R: SA). Contralateral left plantaris muscle was used as sham control (L: Sham).

(E) Body wight, plantaris muscle weight, plantaris muscle weight per body weight, or increased ratio of plantaris muscle weight (SA/Sham) of male control (n=4) or CD47-cKO (n=4) mice.

(F) Representative muscle sections stained with anti-laminin α2 (green) antibody for calculating CSA. Scale bar: 50 μm. The graphs indicate CSA (left) or myonuclear number/myofiber (right) of male control (n=4) or CD47-cKO (n=4) mice.

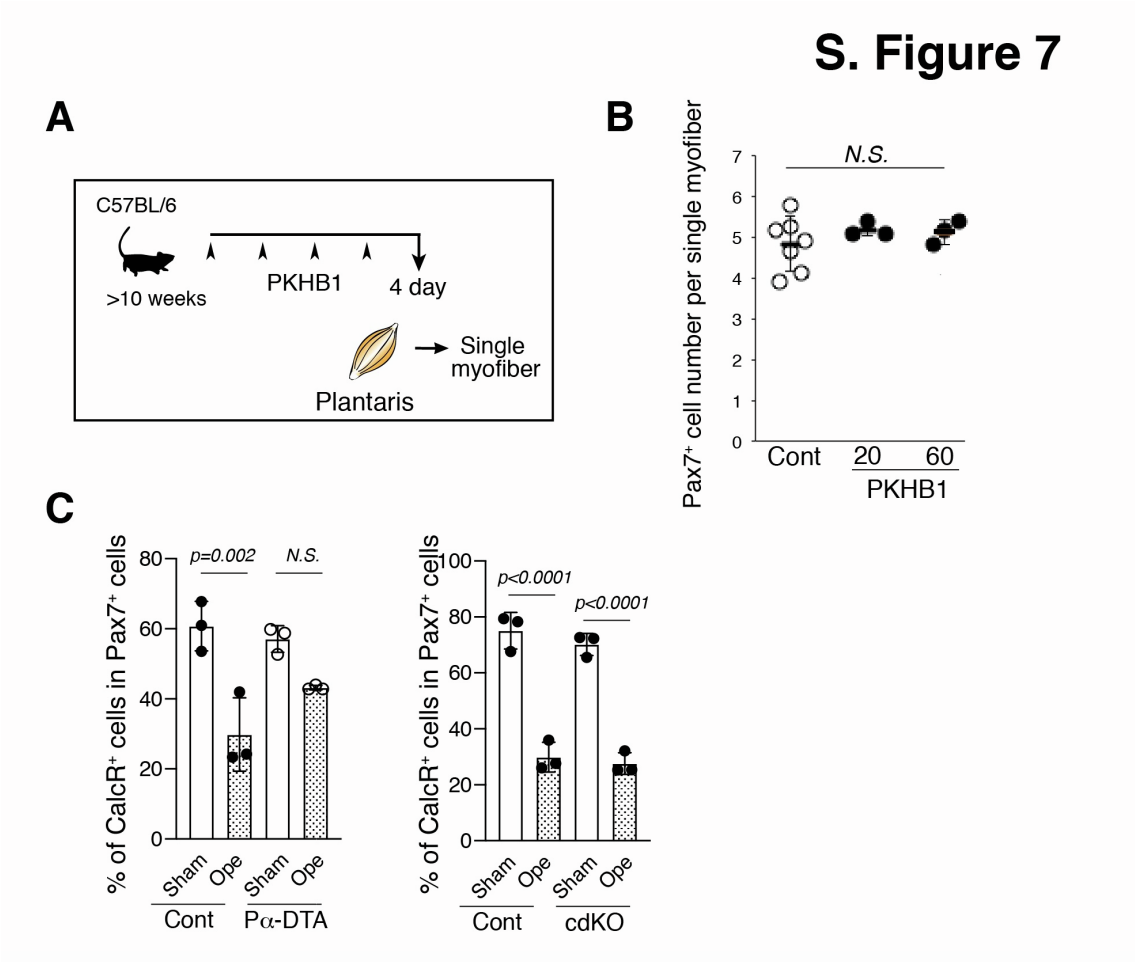

Figure S7. Function of PKHB1 in sedentary C57BL/6 or expression of CalcR in Pα-DTA or Pα-Yap1/Taz -cdKO mice; Related to Figure 7

(A) Experimental scheme for analyzing the effect of CD47 agonist (PKHB1) on myonuclear accretion in sedentary C57BL/6 mice.

(B) The graph indicates the average number of MuSCs on single myofiber of control (PBS-treated, open circle, n=7) and PKHB1-treated mice (20 mg/kg, n=3; 60 mg/kg, n=3). Data are presented as mean ± S.D.; ANOVA. N.S., not significant. 26-30 myofibers were observed per mouse.

(C) Frequency of $Pax7^{+}CalcR^{+}$ MuSC in Sham and Ope muscle of Pα-DTA (left, n=3; two male, one female) or cdKO (right, n=3; three male) mice. Rosa-DTA (n=3; two male,

one female) or *Yap1*$^{flox/flox}$*Taz*$^{flox/flox}$ mice (n=3; three male) were used for each control. 18-30 myofibers were observed for calculating the frequency of CalcR^{+} cell in Pax7 cells per mouse.

Supplementary Table S1: List of genotyping primers used in this study, related to STAR Methods.

Strain	Primer name	Primer sequence
Pax7-CreERT2	Pax7-CE Fwd	ACT AGG CTC CAC TCT GTC CTT C
	Pax7-CE Rev	GCA GAT GTA GGG ACA TTC CAG TG
Calcr-floxed	Calcr loxp Fwd	CAA CTA TAC TCT GTG CAA CGC
	Calcr loxp Rev	TAA TAC GCT TCA GAA ACC
Rosa-DTA	oIMR8052	GCG AAG AGT TTG TCC TCA ACC
	oIMR8545	AAA GTC GCT CTG AGT TGT TAT
	oIMR8546	GGA GCG GGA GAA ATG GAT ATG
CD47-floxed	CD47-F	AGA TAA GGA GGT CCA CTT CT
	CD47-F4	TGA AGC TCC TCA CTC TCC AGT G
	CD47-R2	TGT TCT CTC TGC TCC AGT GCT TAC
Pdgfra-CreERT	pdgfra ex2 (forward)	TCA GCC TTA AGC TGG GAC AT
	cre (reverse)	ATG TTT AGC TGG CCC AAA TG
Yap1-floxed	Yap1Fwd-29878	AGG ACA GCC AGG ACT ACA CAG
	Yap1Rev-29879	CAC CAG CCT TTA AAT TGA GAA C
Taz-floxed	SWg0005 Taz	GGG CAA AGT TGT GAT GCC CTG GAC
	SWg0006 Taz	CCA ATG GCC TGG ATC TCT TAG GGC
Pdgfra-H2B-eGFP	oIMR7801	CCC TTG TGG TCA TGC CAA AC
	oIMR7802	GCT TTT GCC TCC ATT ACA CTG G
	oIMR7919	ACG AAG TTA TTA GGT CCC TCG AC
Rosa-YFP	oIMR8545	AAA GTC GCT CTG AGT TGT TAT
	oIMR4982	AAG ACC GCG AAG AGT TTG TC
	oIMR8546	GGA GCG GGA GAA ATG GAT ATG
Thbs1-KO	oIMR5186	GAG TTT GCT TGT GGT GAA CGC TCA G
	oIMR5187	AGG GCT ATG TGG AAT TAA TAT CGG
	oIMR5188	TGC TGT CCA TCT GCA CGA GAC TAG